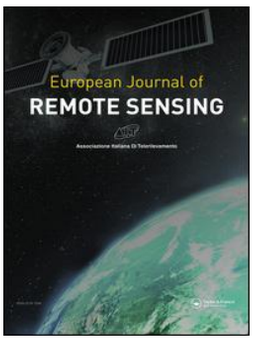

European Journal of Remote Sensing

ISSN: (Print) 2279-7254 (Online) Journal homepage: https://www.tandfonline.com/loi/tejr20

D-RUSLE: a dynamic model to estimate potential soil erosion with satellite time series in the Italian Alps

Marco Gianinetto, Martina Aiello, Francesco Polinelli, Federico Frassy, Maria Cristina Rulli, Giovanni Ravazzani, Daniele Bocchiola, Davide Danilo Chiarelli, Andrea Soncini & Renata Vezzoli

To cite this article: Marco Gianinetto, Martina Aiello, Francesco Polinelli, Federico Frassy, Maria Cristina Rulli, Giovanni Ravazzani, Daniele Bocchiola, Davide Danilo Chiarelli, Andrea Soncini & Renata Vezzoli (2019): D-RUSLE: a dynamic model to estimate potential soil erosion with satellite time series in the Italian Alps, European Journal of Remote Sensing, DOI: 10.1080/22797254.2019.1669491

To link to this article: https://doi.org/10.1080/22797254.2019.1669491

Published online: 26 Sep 2019.

EUROPEAN JOURNAL OF REMOTE SENSING
https://doi.org/10.1080/22797254.2019.1669491

D-RUSLE: a dynamic model to estimate potential soil erosion with satellite time series in the Italian Alps

Marco Gianinetto[a], Martina Aiello[a], Francesco Polinelli[a], Federico Frassy[a], Maria Cristina Rulli[b], Giovanni Ravazzani[b], Daniele Bocchiola[b], Davide Danilo Chiarelli[b], Andrea Soncini[b] and Renata Vezzoli[a]

[a]Department of Architecture, Built Environment and Construction Engineering, Politecnico di Milano, Milano, Italy; [b]Department of Civil and Environmental Engineering, Politecnico di Milano, Milano, Italy

ABSTRACT

Soil erosion is addressed as one of the main hydrogeological risks in the European Union. Since the average annual soil loss rate exceeds the annual average formation rate, soil is considered as a non-renewable resource. Besides, human activities, human-induced forces and climate change have further accelerated the erosion processes. Therefore, understanding soil erosion spatial and temporal trends could provide important information for supporting government land-use policies and strategies for its reduction. This paper describes the Dynamic Revised Universal Soil Loss Equation (D-RUSLE) model, a modified version of the well-known RUSLE model. The RUSLE model formulation was modified to include variations in rainfall erosivity and land-cover to provide more accurate estimates of the potential soil erosion in the Italian Alps. Specifically, the modelling of snow occurrence and the inclusion of Earth Observation data allow dynamic estimation of both spatial and temporal land-cover changes. Results obtained in Val Camonica (Italy) show that RUSLE model tends to overestimate erosion rates in Autumn/Winter because not considering snow cover and vegetation dynamics. The assimilation of satellite-derived information in D-RUSLE allows a better representation of soil erosion forcing, thus proving a more accurate erosion estimate for supporting government land-use policies and strategies for reducing this phenomenon.

ARTICLE HISTORY
Received 18 January 2019
Revised 30 July 2019
Accepted 16 September 2019

KEYWORDS
Satellite time series; NDVI; RUSLE model; soil erosion; natural hazards; Alpine basin

Introduction

Soil is an extremely complex and variable medium and is subject to a series of degradation threats, like erosion, decline in organic matter, local and diffuse contamination and landslides. However, soil formation is such an extremely slow process that soil can be considered as a non-renewable resource (COM (2006) 231 final; Rulli, Offeddu, & Santini, 2013). As an example, the average annual soil loss rate in Europe accounts for 2.46 [t ha^{-1} yr^{-1}] (Panagos et al., 2015a), which is about the double of the average soil formation rate, estimated in 1.4 [t ha^{-1} yr^{-1}] (Verheijen, Jones, Rickson, & Smith, 2009).

According to the European Commission Soil Thematic Strategy, soil erosion is one of the main hydrogeological risks in Europe, where 115 million hectares (12% of Europe's total land area) are subject to water erosion. Besides, human activities, human-induced forces and climate change have slightly shown an effect in accelerating soil loss (COM (2006) 231 final; Rosso, Rulli, & Bocchiola, 2007). Among all European regions, the Mediterranean countries, with the Alps in particular, have the highest soil loss rates due to special climatic conditions with prolonged dry periods followed by heavy rainfall combined with steep slopes (Panagos et al., 2015a).

Soil erosion is defined as the detachment of soil particles caused by the locally intense shear stress generated by raindrop impact (Merritt, Letcher, & Jakeman, 2003). Thus, from a modelling point of view erosion is mainly controlled by precipitation, topography, soil properties, land use/land cover and soil conservation practices. An ideal model would describe all the individual processes on the basis of hydraulics, hydrology and sediment transport theory equations, providing the basin response in terms of volume of sediments passing through the closing section for a given input rainfall. However, nowadays there are many simplified models in the literature.

Based on their constitutive framework, erosion models can be grouped in: i) empirical models; ii) conceptual models and iii) physics-based erosion and sediment transport models.

Empirical models do not depend on a rigorous description of the physical process and require less computational cost and less a priori information. While being simple models, still they are useful tools for estimating soil loss at a catchment scale when limited data and input parameters are available (Merritt et al., 2003). The most widely used empirical models are USLE (*Universal Soil*

CONTACT Marco Gianinetto marco.gianinetto@polimi.it Department of Architecture, Built Environment and Construction Engineering, Politecnico di Milano, Milano, Italy

Loss Equation) (Wischmeier & Smith, 1978), MUSLE (*Modified Universal Soil Loss Equation*) (Williams, 1975), RUSLE (*Revised Universal Soil Loss Equation*) (Renard, Foster, Weesies, McCool, & Yoder, 1997), AGNPS (*AGricultural Non-Point Source pollution model*) (Young, Onstad, Bosch, & Anderson, 1989) and SEDD (*SEdiment Delivery Distributed*) (Ferro & Porto, 2000).

Conceptual models describe the watersheds with a series of storage units and incorporate the general description of the catchment dynamics in terms of the underlying processes of sediment and runoff generation (Merritt et al., 2003). Some examples are CREAMS (*field scale model for Chemicals, Runoff and Erosion from Agricultural Management Systems*) (Knisel, 1980) and LASCAM (*LArge Scale CAtchment Model*) (Viney & Sivapalan, 1999).

Finally, physically based erosion and sediment transport models use the mass conservation equation for flow and sedimentation processes simulation. They are able to describe the different phenomena contributing to erosion and their interactions, simultaneously (Merritt et al., 2003; Rulli & Rosso, 2005). The rigorous description of the physical processes makes possible to extend their use to areas with very different characteristics. Although providing a more realistic representation of the processes, these models can suffer from high uncertainty due to a large number of input parameters required, that often need to be calibrated against observed data (Merritt et al., 2003). Some examples are EUROSEM (*EUROpean Soil Erosion Model*) (Morgan et al., 1998), WEPP (*Water Erosion Prediction Project*) (Laflen, Lane, & Foster, 1991) and ANSWERS (*Areal Non point Source Watershed Environment Response Simulation*) (Beasley, Huggins, & Monke, 1980).

Soil erosion models are important tools for understanding soil loss rates, spatial patterns and trends for supporting government land-use strategies for effective erosion control practices and soil conservation (Igwe, Onuigbo, Chinedu, Ezeaku, & Muoneke, 2017). Even if the factors that influence erosion could be extremely variable in time and space, nonetheless these models frequently use a static definition for some of the input parameters that may present changes in space and time such as land cover. Therefore, Earth Observation can help improving results (Aiello, Adamo, & Canora, 2015).

In past years, multispectral satellite images were adopted to detect erosion features and eroded areas (e.g. large and medium-sized gullies and badlands) or erosion consequences (e.g. water quality assessment in terms of suspended sediments in reservoirs and lakes) (Vrieling, 2006). Land-cover mapping is a common input for soil erosion modelling because different land classes have a different protective effect towards erosion, especially vegetation (Feoli, Vuerich, & Zerihun, 2002). Once mapped, vegetation is assigned a sheltering effect, depending on its type (Vrieling, 2006; Wischmeier & Smith, 1978) or based on a vegetation index (Flügel, Märker, Moretti, Rodolfi, & Sidrochuk, 2003; Van der Knijff, Jones, & Montanarella, 1999).

The main advantage of using satellite Remote Sensing data within soil erosion studies is the ability to account for seasonal variability of vegetation, long-term land-cover changes and to provide such information with a spatial resolution suitable to exploit soil erosion at regional/local scale. Of course, optical data suffer from a lack of information in case of cloud cover and shadows, which are relevant in the mountainous environment and especially during the Winter. Nevertheless, the actual high revisit time compensates this issue.

In this work, we model the potential soil erosion rate, at the catchment scale, in the central alpine and pre-alpine area of Italy by integrating a modified version of the RUSLE model (Renard et al., 1997) with multi-temporal satellite observations. RUSLE is widely used in the scientific community (Beskow et al., 2009; Fernandez, Wu, McCool, & Stöckle, 2003) and is usually applied considering the average rainfall erosivity, no land-use /land-cover changes and, thus, static sheltering effect provided by vegetation within the simulation period. Here we introduce (i) the seasonal dynamics of precipitation by considering both rainfall (active in erosion) and snow (non-contributing to erosion); (ii) the sheltering effect of snow cover dynamics; (iii) the seasonal dynamics of vegetated areas and (iv) long-term land-use/land-cover changes. All these novelties aim to improve potential soil erosion modelling in the Alps. To provide an indication of the reliability of D-RUSLE outputs at large scale, we provide a comparison with a recent reference dataset available for Europe (Panagos et al., 2015a), while the application of an inflow coefficient to D-RUSLE outputs allows a comparison against the results of two plot scale erosion experiments pursued within the study area under controlled rainfall.

Study area

This study estimates the potential soil erosion in the central alpine and pre-alpine area of Italy. The study area is Val Camonica (one of the largest valleys of the Central Alps), that is the Oglio River basin closed at Sarnico, which extends about 1,800 km^2 (Figure 1(a)).

Altitudes range from 185 [m a.s.l.] in Sarnico to 3,585 [m a.s.l.] of the Adamello Glacier. Here, we divided the study area in three altitude ranges (Figure 1(b)): high elevation areas (elevation ≥ 1,600 [m a.s.l.]), medium elevation areas (1,000 [m a.s.l.] < elevation < 1,600 [m a.s.l.]) and Lake Iseo areas (elevation ≤ 1,000 [m a.s.l.]).

Considering geology of the study area, the upper and the western portion are characterized by a complex of

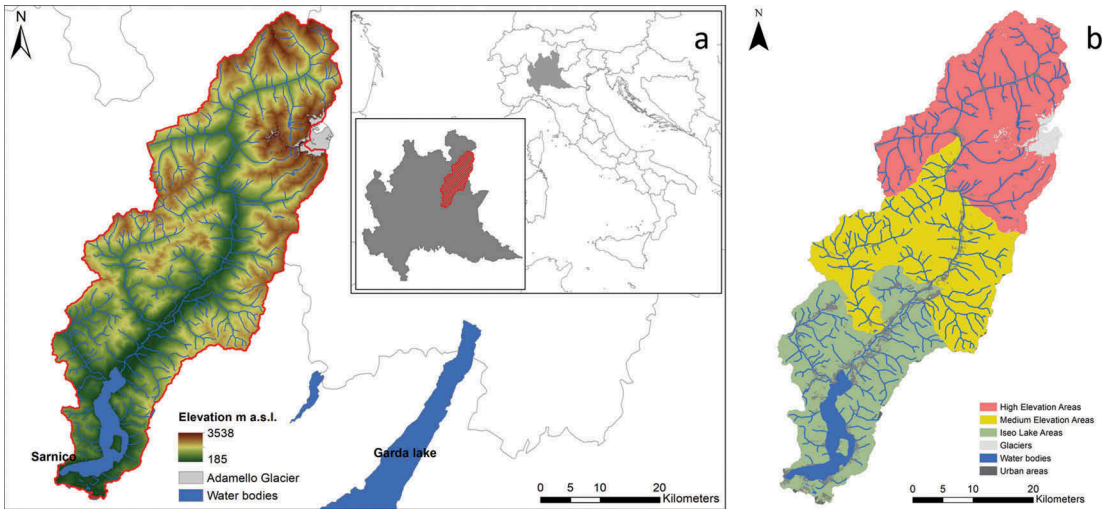

Figure 1. Study area: (a) digital elevation model of val camonica; (b) subdivision of the study area in high elevation areas (elevation ≥ 1,600 [m a.s.l.]), medium elevation areas (1,000 [m a.s.l.] < elevation < 1,600 [m a.s.l.]) and Lake Iseo areas (elevation ≤ 1,000 [m a.s.l.]).

igneous and metamorphic rocks, while the remaining portion is characterised by a complex of calcareous sedimentary rocks.

Almost 90% of the landscape is vegetated (about 45% are forests and only less than 1% are croplands), characterized by the typical mountainous vegetation distribution with altitude and influenced by precipitation seasonal regimes.

Val Camonica is characterized by an alpine climate, with cold Winter (average temperature 1.16 [°C]) and moderate Summer temperatures (average temperature 18.3 [°C]). The annual average precipitation is about 1,300 [mm yr^{-1}], with peaks in the Summer and Autumn. Snowfall is possible from October to May and the snow cover generally persists at higher altitudes until July.

Data

Within this work, we refer to official data supplied by Regione Lombardia (www.geoportale.regione.lombardia.it/), Comunità Montana della Valle Camonica (www.geoportale.cmvallecamonica.bs.it/) and Environmental Protection Agency of Regione Lombardia (www.arpalombardia.it/siti/arpalombardia/meteo), which are available in their geo-portals.

Thematic maps

With regard to thematic maps, we used:

- The 30-m spatial resolution Digital Elevation Model of Regione Lombardia (Figure 1);
- The DUSAF (*Destinazione d'Uso dei Suoli Agricoli e Forestali*) land-cover/land-use map of Regione Lombardia for the years 2000, 2007 and 2015. This thematic map is organized in five hierarchical levels where the first three are compliant with the European Corine Land Cover (CLC) map. Additional land-cover/land-use classes representative of Regione Lombardia territory are also available. Within this work, we used the third level, because C-Factor values (or range of values) are provided in literature for land-cover classes discretized at that level of description, sufficient to take into account the land-cover variability in space and time (Figure 2);
- The soil map of Regione Lombardia (Figure 3).

Meteorological data

With regard to meteorological data, we used hourly time series of precipitation and air temperature recorded from 2003 to 2017 by 30 rain gauges and 28 thermometers belonging to the Environmental Protection Agency of Regione Lombardia (Figure 4).

Remote sensing data

With regard to Remote Sensing data, we used a time series made of 20 images collected by Landsat-5/TM, Landsat-7/ETM+ and Landsat-8/OLI in the period 2002–2017. The images were acquired both in Autumn/Winter (September–February) and in Spring/Summer (March–August) to provide seasonal estimates.

Field survey

In the Summer 2017, we collected 13 soil samples in the North East of the study area, where the elevation is higher

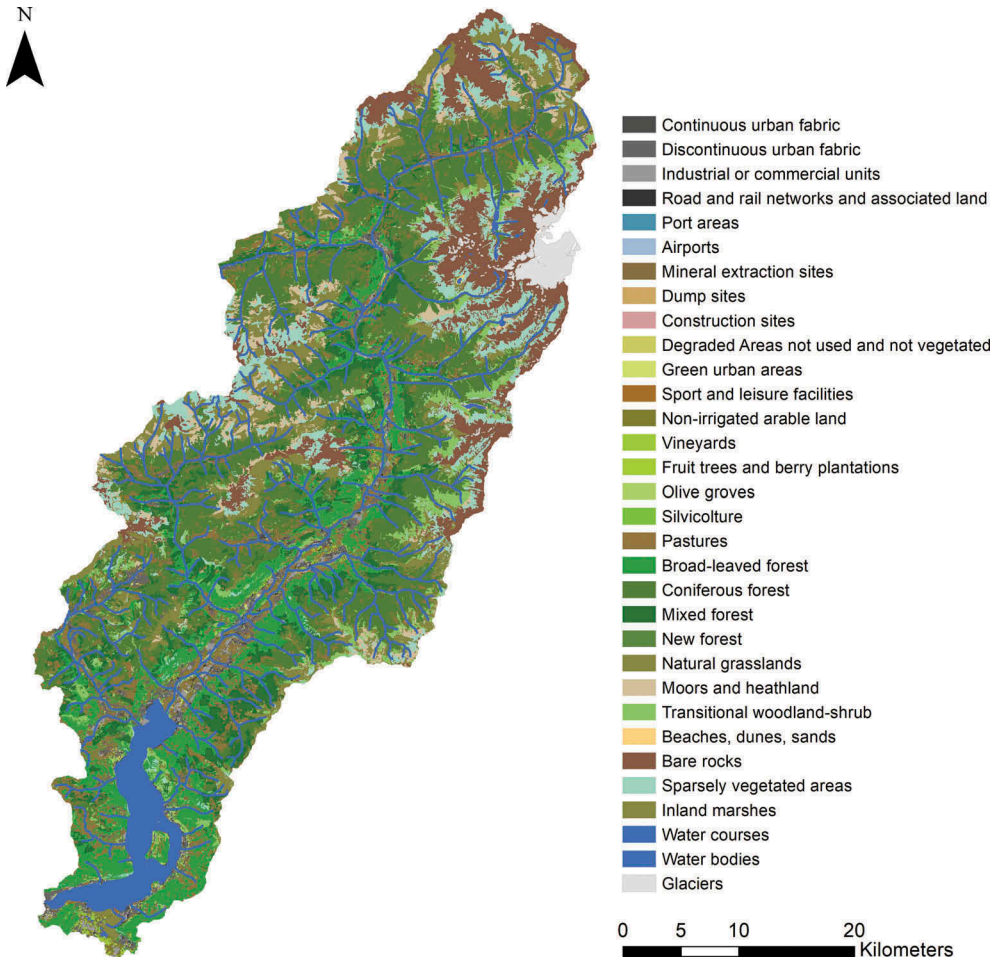

Figure 2. The DUSAF (*Destinazione d'Uso dei Suoli Agricoli e Forestali*) land-cover/land-use map of regione lombardia for the year 2015.

and rocks are mainly metamorphic. In the Summer 2018, we collected 14 soil samples at the lower altitudes of South West, where there is a predominance of calcareous sedimentary rocks. Sampling plots were selected to maximize soil texture and taxonomy variability within the study area (Figure 5).

The particle size distribution of the soil sample collected at *Case di Viso* was also used for validation (refer to section "5.2 Comparison with plot scale erosion experiments").

Methods

Standard modelling of potential soil erosion

The empirical Revised Universal Soil Loss Equation (RUSLE) is a very popular model to estimate the annual potential soil erosion rate due to rainfall (Renard et al., 1997). Although originally developed for agricultural application, today RUSLE is used as a general model to provide estimates also for non-agricultural lands at different spatial scales, even at continental scale (Panagos et al., 2015a).

RUSLE estimates the annual potential soil erosion rate E [t ha^{-1} yr^{-1}] through five parameters, as shown in Equation (1):

$$E = R \times K \times LS \times C \times P \quad (1)$$

where:

R is the rainfall erosivity [MJ mm ha^{-1} h^{-1} yr^{-1}], also called R-factor, which is the driving force of erosion and is a function of precipitation rate, air temperature and snow cover dynamics;

K is the soil erodibility [t ha h ha^{-1} MJ^{-1} mm^{-1}], also called K-factor, which describes the soil properties (i.e. soil structure and organic matter content) that influence the predisposition of soil to erosion;

LS [-] is a dimensionless combined parameter, also called LS-factor, that describes the impact of slope length and slope steepness on soil erosion;

C [-] is a dimensionless parameter, also called C-factor, that describes how land-use and land-cover protect the soil from erosion (lower C-factor values correspond to higher protection, thus to lower erosion);

P [-] is a dimensionless parameter, also called P-factor, that describes the impact of soil conservation practices to reduce the potential erosion.

We used precipitation data to estimate the daily rainfall erosivity at each rain gauge with the Rainfall Intensity Summarization Tool (RIST) code (USDA, 2018). Then, rainfall erosivity was aggregated at

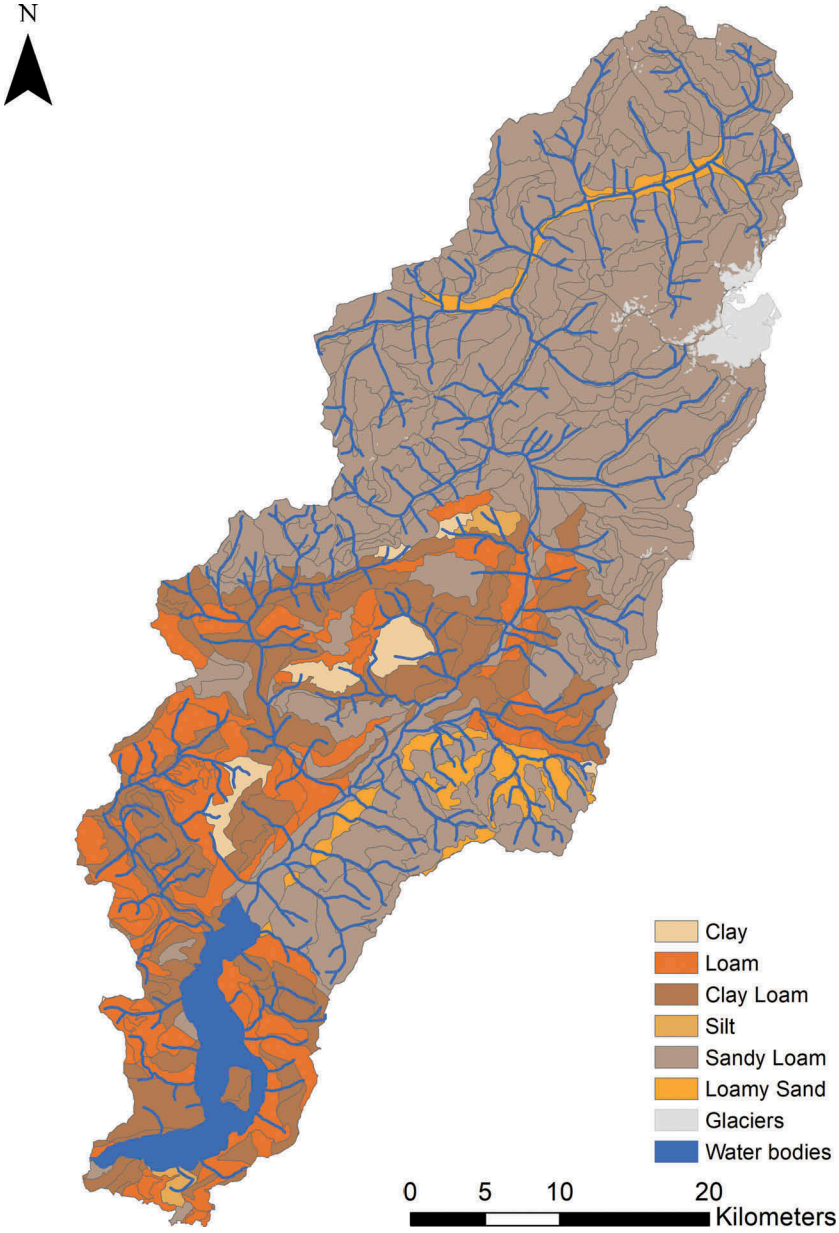

Figure 3. Soil map of the study area.

a monthly scale and spatialized on a 30 [m] grid with the inverse-square law, as shown in Figure 6(a) (R1).

When organic matter content, texture, structure and permeability are known, soil erodibility can be estimated with Equations (2–3) (Renard et al., 1997; Wischmeier & Smith, 1978):

$$K = \frac{2.1 \times 10^{-4} \times M^{1.14}(12 - OM) + 3.25 \times (s - 2) + 2.5 \times (p - 3)}{100} \times 0.1317 \quad (2)$$

where:

OM [%] is the organic matter content;

s is the soil structure class (*s* = 1: very fine granular, …, *s* = 4: blocky, platy or massive);

p is the permeability class (*p* = 1: very rapid, …, *p* = 6: very slow).

and *M* is the textural factor computed as:

$$M = \left(M_{silt} + M_{vfs}\right) \times (100 - m_c) \quad (3)$$

where:

m_c [%] is the fractional content of clay (particle size < 0.002 [mm]);

m_{silt} [%] is the fractional content of silt (0.002 [mm] ≤ particle size < 0.05 [mm]);

m_{vfs} [%] is the fractional content of very fine sand (0.05 [mm] ≤ particle size < 0.1 [mm]).

Detailed information concerning soil texture was not available for our study area; therefore, we resampled the K-factor map made by JRC (Panagos, Meusburger, Ballabio, Borrelli, & Alewell, 2014) from its 500 [m] spatial resolution to 30 [m] spatial resolution (Figure 6(b)) (K1).

In the literature, we can find several different formulations for estimating the LS-factor. Quite commonly used it is the equation proposed by Mitasova,

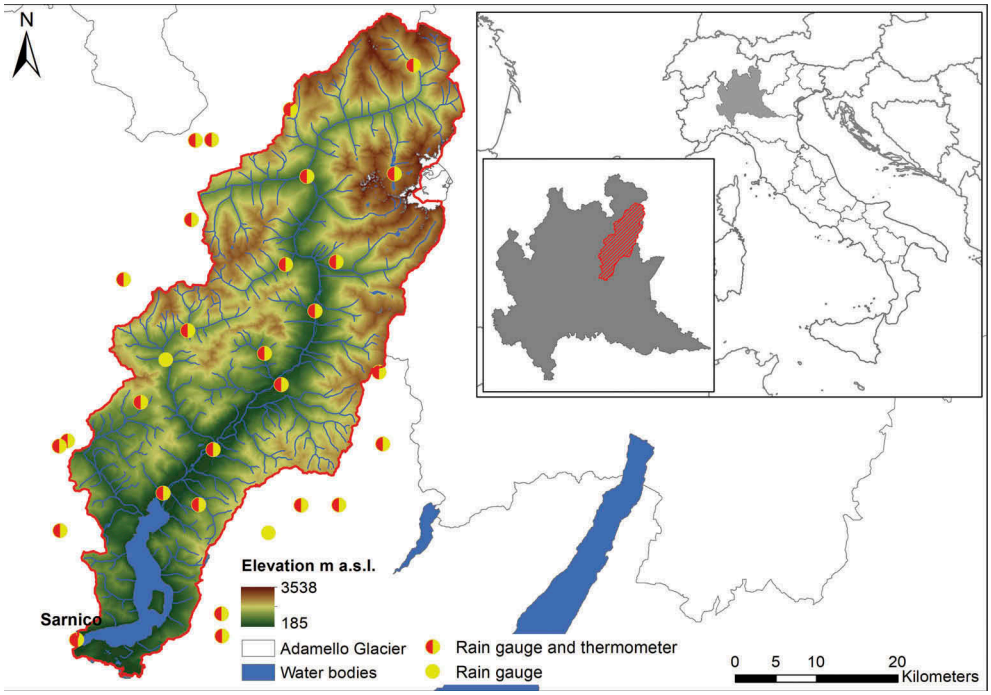

Figure 4. Study area with highlighted the rain gauges and the thermometers used.

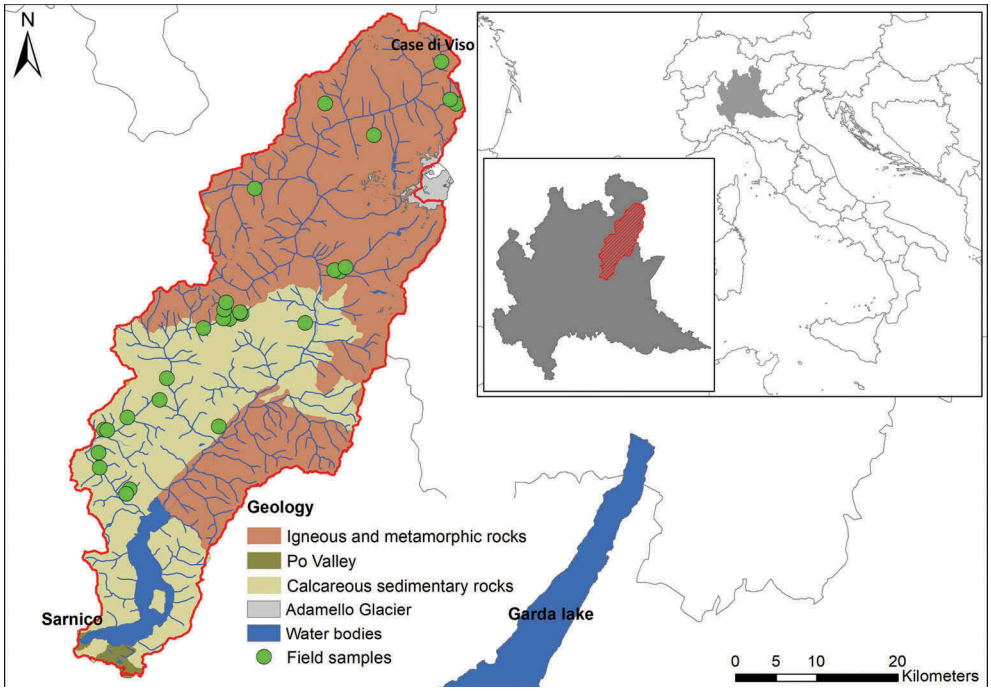

Figure 5. Geology of the study area, with highlighting of the sampling plots.

Hofierka, Zlocha, and Iverson (1996), which takes into account the unitary catchment area as input in each cell:

$$LS = (m+1)\left(\frac{U_{in}}{22.13}\right)^{m}\left(\frac{\sin(\theta)}{\sin(5^{\circ})}\right)^{n} \quad (4)$$

where:

U_{in} m^2 m^{-1} is the contributing area to the cell for perimeter unit;

22.13 [m] is the length of the RUSLE standard parcel;

θ [°] is the cell slope;

5 [°] is the slope of the RUSLE standard parcel;

m and n are empirical coefficients (in literature typical values are $0.4 \leq m \leq 0.6$ and $1.0 \leq n \leq 1.3$).

In this study, we used m = 0.4 and n = 1.3. Figure 6(c) shows the map for LS-factor (LS1).

In traditional RUSLE each land-cover class is assigned a unique and static C-factor, usually retrieved from literature. In this work, the C-factor is assigned using the DUSAF land-cover/land-use map of 2015 and tabulated data extracted from

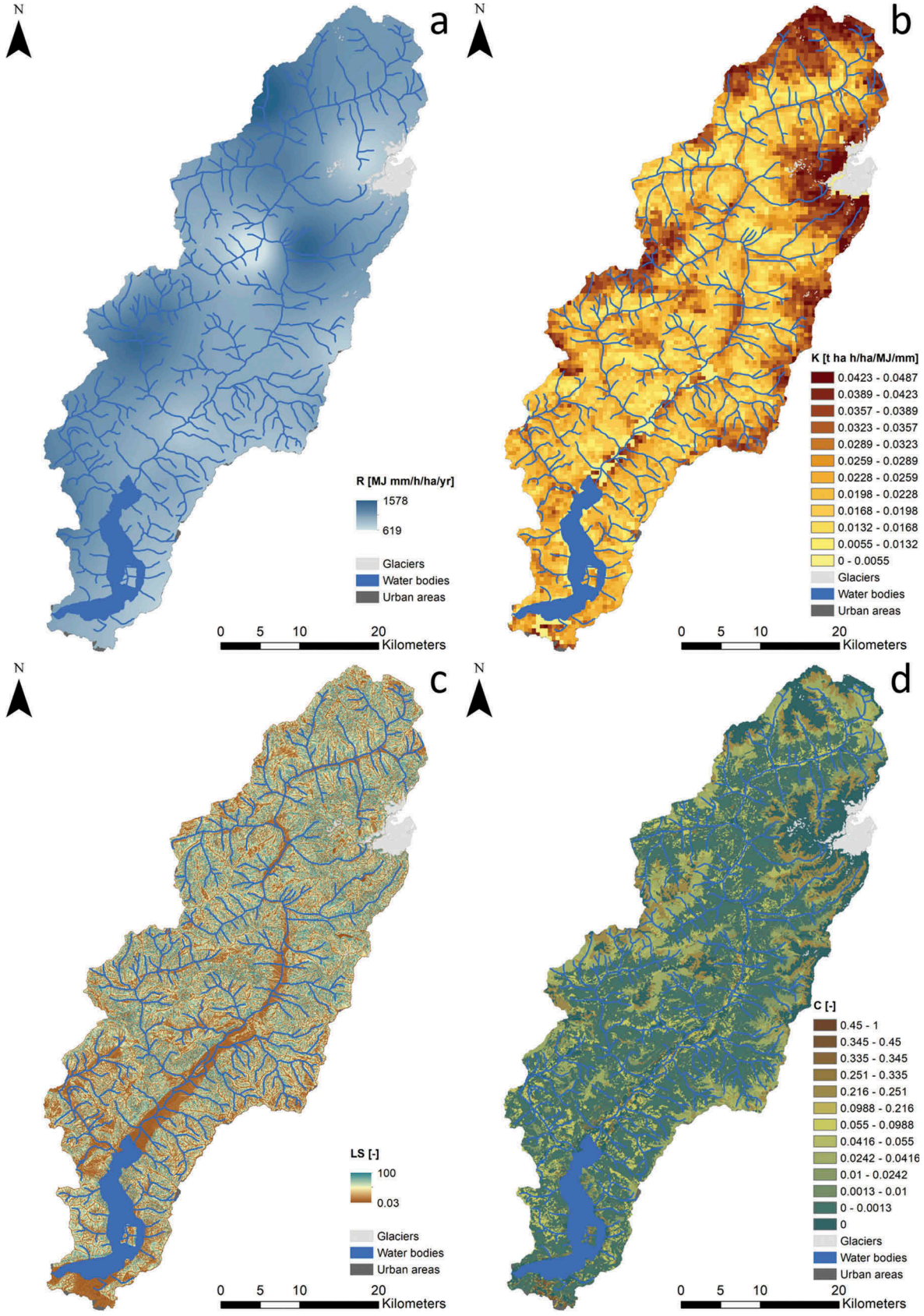

Figure 6. Parameters of classic RUSLE: (a) rainfall erosivity (R1 parametrization); (b) soil erodibility (K1 parametrization); (c) slope length and steepness (LS1 parametrization); (d) cover management type (C0 parametrization).

Panagos et al. (2015b) and Bosco, Rusco, Montanarella, and Panagos (2009) as summarized in Gianinetto et al. (2018) (C0). Table 1 reports the correspondences between land-cover classes and C-factor and Figure 6(d) shows its geographic distribution.

Table 1. Tabulated C-factor values assigned to each DUSAF land-cover classes (column "C-factor

Table 1. Tabulated C-factor values assigned to each DUSAF land-cover classes (column "C-factor (DUSAF)") and tabulated C-factor ranges for each DUSAF land-cover classes (column "C-factor range") (Gianinetto et al., 2018). C-factor value sources are (a) the parametrization proposed for Italy by Panagos et al. (2015), the central value of the C-factor range values for Europe from (b) Panagos et al. (2015) or (c) Bosco et al. (2009).

Land-cover class name	Land-cover class code	C-factor (DUSAF)	C-factor range
Continuous urban fabric	111	0.00000	0.00
Discontinuous urban fabric	112	0.00000	0.00
Industrial or commercial units	121	0.00000	0.00
Road and rail networks and associated land	122	0.00000	0.00
Port areas	123	0.00000	0.00
Airports	124	0.00000	0.00
Mineral extraction sites	131	0.00000	0.00
Dump sites	132	0.00000	0.00
Construction sites	133	0.00000	0.00
*Degraded Areas not used and not vegetated	134	0.00000	0.00
Beaches, dunes, sands	331	0.00000$_{(b)}$	0.00
Bare rocks	332	0.00000$_{(b)}$	0.00
Glaciers and perpetual snow	335	0.00000$_{(b)}$	0.00
Water course	511	0.00000	0.00
Water bodies	512	0.00000	0.00
Green urban areas	141	0.00100$_{(c)}$	
Inland marshes	411	0.00100$_{(c)}$	
*Silvicolture	224	0.00130$_{(a)}$	
Broad-leaved forest	311	0.00130$_{(a)}$	0.0001–0.003
Coniferous forest	312	0.00130$_{(a)}$	0.0001–0.003
Mixed forest	313	0.00130$_{(a)}$	0.0001–0.003
*New forest	314	0.00130$_{(a)}$	
Sport and leisure facilities	142	0.01000$_{(c)}$	
Transitional woodland-shrub	324	0.02420$_{(a)}$	0.003–0.05
Natural grasslands	321	0.04160$_{(a)}$	0.01–0.08
Moors and heathland	322	0.05500$_{(b)}$	0.01–0.1
Pastures	231	0.09880$_{(a)}$	0.05–0.15
Fruit trees and berry plantations	222	0.20000$_{(b)}$	0.1–0.3
Olive groves	223	0.21630$_{(a)}$	0.1–0.3
Sparsely vegetated areas	333	0.25090$_{(a)}$	0.1–0.45
Non-irrigated arable land	211	0.33500$_{(b)}$	
Vineyards	221	0.34540$_{(a)}$	0.15–0.45

*not in Corine Land Cover classification

(DUSAF)") and tabulated C-factor ranges for each DUSAF land-cover classes (column "C-factor range") (Gianinetto et al., 2018). C-factor value sources are (a) the parametrization proposed for Italy by Panagos et al. (2015b), the central value of the C-factor range values for Europe from (b) Panagos et al. (2015b) or (c) Bosco et al. (2009).

Finally, it is very difficult to define P-factor. In facts, although few authors tried to estimate the P-factor from land-cover information, this parameter is usually not considered in erosion studies because its estimation needs a very detailed knowledge of local soil management practices. Consequently, we set P = 1.

The dynamic RUSLE model

RUSLE model was originally developed for the estimation of soil loss in flat agricultural areas. While retaining the same formal equation of the original RUSLE (Renard et al., 1997), we propose an alternative parametrization called Dynamic RUSLE (D-RUSLE). D-RUSLE includes the effects of rainfall intensity, snow cover dynamics and land-cover/land-use changes in time, thus reflecting more realistically precipitation erosivity and the sheltering effect of snow and vegetation seasonal dynamics.

Hourly measured rainfall data are spatialized with the inverse-square law on a 30 [m] grid. To obtain temperature hourly data on a regular grid 30 [m] the procedure is more complex than for precipitation since it requires to: (1) estimate the observed hourly temperature gradient; (2) apply a linear regression to project observed temperature to 1000 [m a.s.l.] altitude; (3) spatialize the temperature at 1000 [m a.s.l.] with the inverse-square law on a 30 [m] grid; (4) apply a linear regression to project the 30 [m] gridded temperature the soil altitude.

Once hourly 30 [m] gridded precipitation and temperature data are available the R-factor (R2) is computed using the equation proposed by Sun, Cornish, and Daniell (2002), with erosion rate expressed in [t ha^{-1} month^{-1}], instead of [kg m^{-2} month^{-1}] (Aiello et al., 2018b):

$$R = \sum_{t=1}^{n_h} 0.138 \times i_{e,t}^2 \quad (5)$$

where:

$i_{e,t}$ [mm h^{-1}] is the effective hourly intensity of precipitation;

n_h is the monthly number of hours.

$$SWE_t = SWE_{t-1} + \begin{cases} +\min\left\{\max\left\{0; \frac{T_{\sup}-T_t}{T_{\sup}-T_{\inf}}\right\}; 1\right\} \times \mathrm{i}_t \text{ IF } i_t > 0, \\ -\min\{\max\{0; C_m \times (T_t - T_m)\}; SWE_{t-1}\} \text{ IF } i_t = 0 \end{cases} \quad (6)$$

The effective hourly intensity of precipitation $i_{e,t}$ is computed with Equations (6–7):

$$i_{e,t} = \begin{cases} 0 \text{ IF } SWE_t > 0 \\ i_t \text{ IF } SWE_t = 0 \end{cases} \quad (7)$$

where:

SWE_t [mm] is the snow water equivalent;

T_t [°C] is the air temperature;

T_{inf} [°C] is the temperature below all the precipitation is snow ($T_{inf} = -3$ [°C]);

T_{sup} [°C] is the temperature above all the precipitation is rain ($T_{sup} = 0$ [°C]);

T_m [°C] is the temperature above snow melting starts ($T_m =$ [°C]);

i_t [mm h^{-1}] is the measured precipitation by the rain gauge (= rain+snow);

C_m [mm h^{-1}°C^{-1}] is the snow melting rate ($C_m = 0.18$ [mm h^{-1}°C^{-1}]).

Equation (6) describes the snow water equivalent dynamics in terms of accumulation (when $i_t > 0$) and melting (when $i_t = 0$), which is used as a proxy for snow cover dynamics. Equation (7) provides the estimated effective hourly intensity of precipitation (i_e) as a function of precipitation, air temperature and snow cover (Figure 8(a)).

The K-factor (K2) is assigned to the different soil textural classes derived from the official soil map of Regione Lombardia according to information retrieved from literature (Fantappiè, Priori, & Costantini, 2015), after local validation (Figure 7). For the 27 soil samples, we measured total organic carbon (TOC), acidity (pH) and texture. Then, we compared the laboratory results with the information extracted from the soil map (here texture is expressed as texture classes). Since we got reasonably good accordance, we assigned each cell a K-factor value based on its TOC and texture class provided by the soil map, according to Table 2; Figure 8(b) reports the spatial distribution of K-factor values.

The LS-factor (LS2) is estimated with the terrain analysis/hydrology module available in SAGA

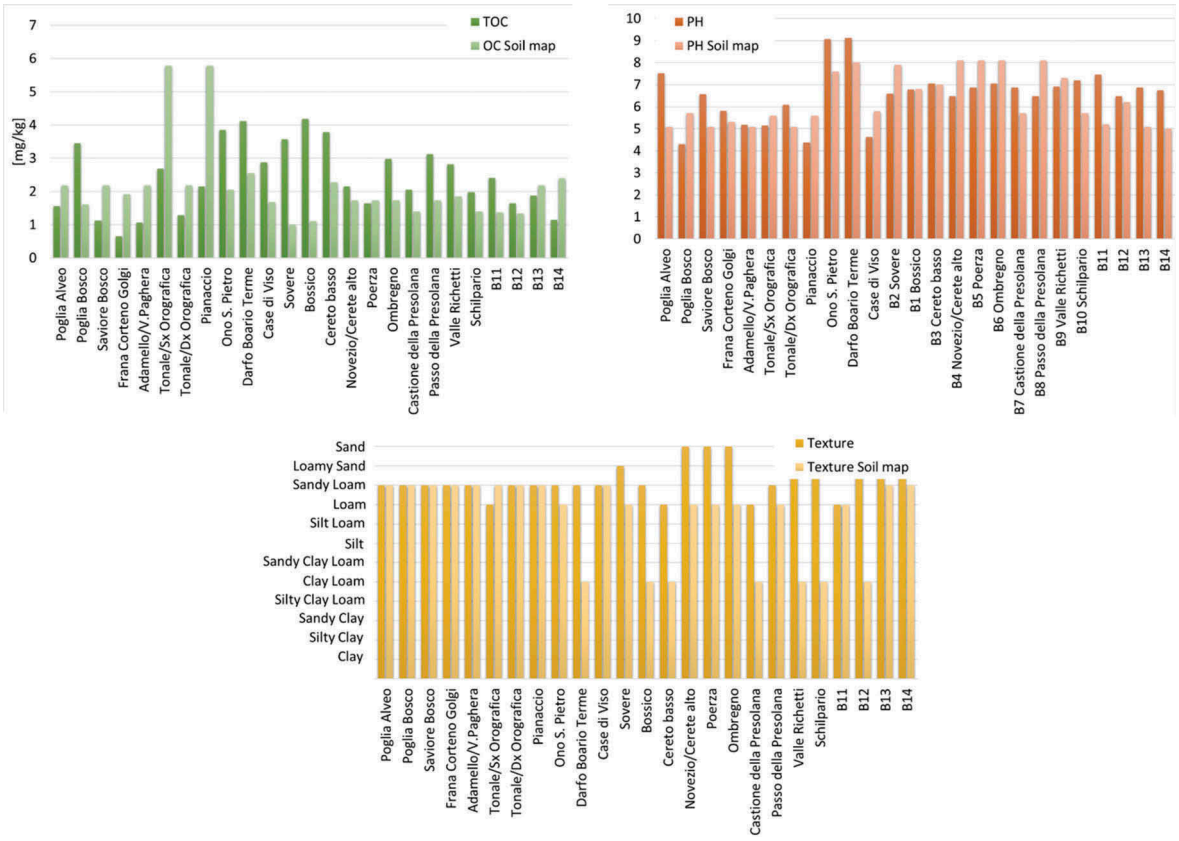

Figure 7. Comparison between TOC, pH and textural class measured for the 27 soil samples and retrieved from the soil map of Regione Lombardia.

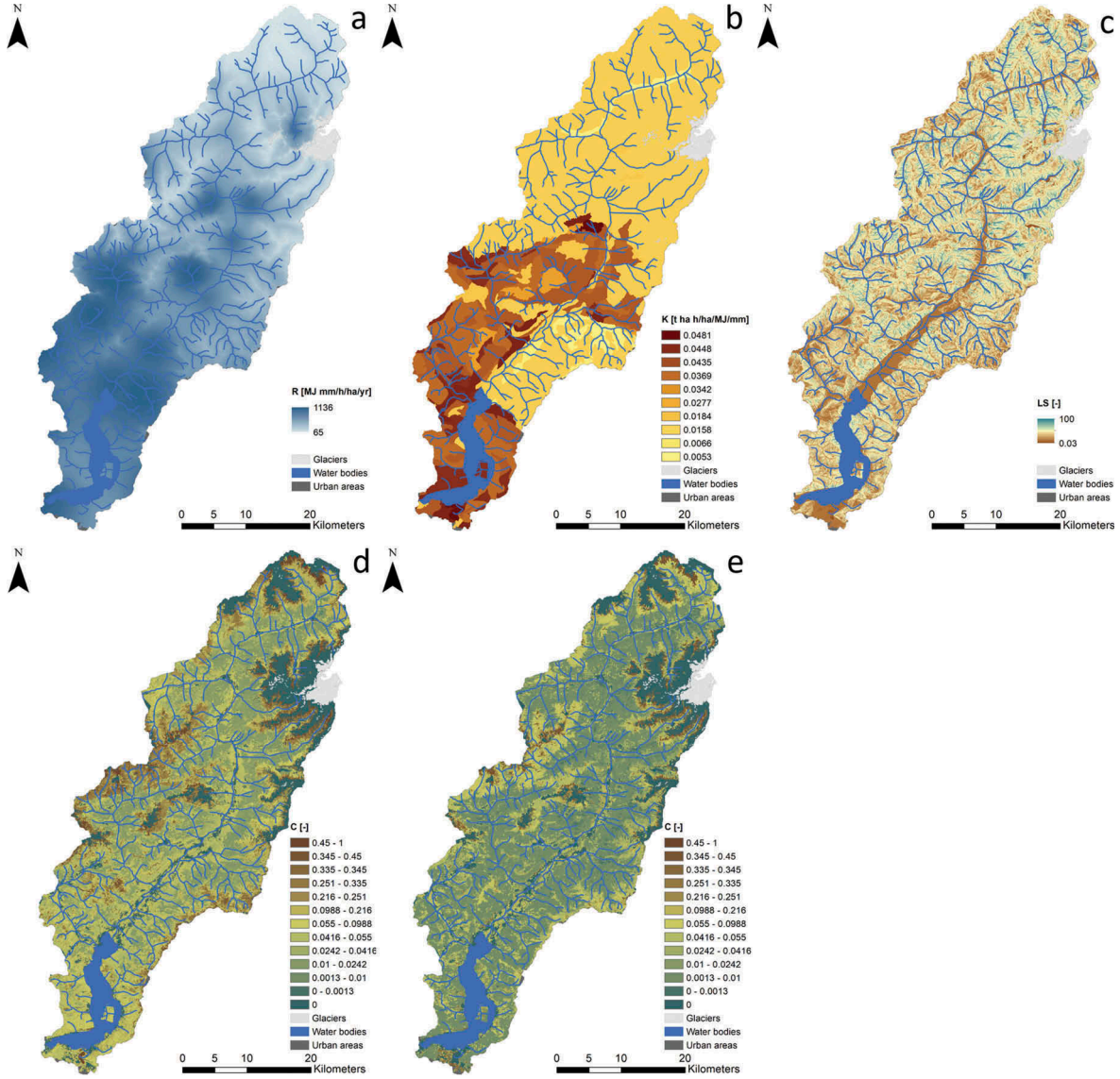

Figure 8. Parameters of D-RUSLE: (a) rainfall erosivity (R2 parametrization); (b) soil erodibility (K2 parametrization); (c) slope length and steepness (LS2 parametrization); (d) cover management type (C1 parametrization); (e) cover management type (C2 parametrization).

Table 2. K-factor values for different textural classes and TOC content (modified from Fantappiè et al. (2015)).

	K-factor	
Soil Texture Classes	For TOC < 1.16 [%]	For TOC > 1.16 [%]
Sand	0.0040	0.0013
Loamy sand	0.0066	0.0053
Sandy loam	0.0184	0.0158
Loam	0.0448	0.0342
Silt loam	0.0540	0.0487
Silt	0.0561	0.0514
Sandy clay loam	0.0263	0.0263
Clay loam	0.0435	0.0369
Silty clay loam	0.0461	0.0395
Sandy clay	0.0277	0.0277
Silty clay	0.0356	0.0342
Clay	0.0316	0.0277

(System for Automated Geoscientific Analyses) that use the popular formulation proposed by Desmet and Govers (1996) (Figure 8(c)). Equation (8) takes into account flow accumulation from upslope cells:

$$LS = \frac{(A_{in} + D^2)^{\left(\frac{\beta}{\beta+1}+1\right)} - A_{in}^{\left(\frac{\beta}{\beta+1}+1\right)}}{x^{\left(\frac{\beta}{\beta+1}\right)} \times 22.13^{\left(\frac{\beta}{\beta+1}\right)} \times D^{\left(\frac{\beta}{\beta+1}+2\right)}} \times S \quad (8)$$

$$\beta = \frac{\frac{\sin(\theta)}{\sin(5^\circ)}}{0.56 + 3 \times [\sin(\theta)]^{0.8}} \quad (9)$$

$$x = |sen(a)| + |cos(a)| \quad (10)$$

$$S = \begin{cases} 10.8 \times \sin(\theta) + 0.03 \text{ IF } \theta < 5[^\circ] \\ 16.8 \times \sin(\theta) - 0.5 \text{ IF } \theta \geq 5[^\circ] \end{cases} \quad (11)$$

where:

A_{in} [m^2] is the contributing area to the cell;
D [m] is the cell size;
22.13 [m] is the length of the RUSLE standard parcel
a [°] is the cell orientation (aspect);
θ [°] is the cell slope.
5 [°] is the slope of the RUSLE standard parcel.

Finally, C-factor is estimated at 30 [m] spatial resolution as a dynamic variable using only satellite Remote Sensing data (C1) and aggregating satellite Remote Sensing data with land-cover maps (C2). Compared to the classic "static" modelling of the cover management factor (C0), satellite data allow the inclusion of its seasonal and inter-annual dynamics.

When no information on land cover is available, C-factor could be estimated from NDVI using Equation (12) proposed by Van der Knijff et al. (1999) (C1), as shown in Figure 8(d):

$$C = e^{-\alpha \times \frac{NDVI}{(\beta - NDVI)}} \tag{12}$$

where:

α and β are empirical coefficients (suggested values for Italy are α and β).

However, it is known (Van der Knijff et al., 1999) that Equation (12) might result in unreliable overestimations of C-factor (i.e. underestimation of the sheltering effect of vegetation) when NDVI is less than 0.65, which could, in turn, reflect into a biased overestimation of soil erosion rates. Moreover, satellite images collected over mountain areas in the Winter have very large shadows, which lead to unreliable estimation of NDVI, thus unreliable estimation of C-factor and, finally, of erosion rates. For those reasons, Equation (12) seems not suitable to study soil erosion in mountain areas.

Here we propose a new method for the estimation of C-factor based on NDVI time series, where information on land cover is used as a priori knowledge to constrain C-factor values (Aiello et al., 2018a) (C2). Satellite images are pre-processed through standard radiometric calibration and atmospheric corrections for non-flat terrain. All the images are grouped into two macro-seasons: Spring/Summer (from March to August) and Autumn/Winter (from September to February), and snow cover and clouds were masked. The study area, as most of the Alpine environment, is characterized by the presence of many steep and narrow valleys and during Autumn/Winter almost half of the territory is completely shadowed or snow-covered. This may result in the ability to produce undersaturated data (i.e. null values in shadowed areas) or oversaturated data (i.e. flat values in snowy areas). For this reason, Autumn/Winter NDVI values were unreliable and thus replaced with synthetic values reconstructed combining Spring/Summer observations and DUSAF land-cover classes. For each Autumn/Winter image, we selected the closest Spring/Summer image and the closest DUSAF among the three maps available. Then, we calculated the pixel-based ratio between Autumn/Winter NDVI and Spring/Summer NDVI, excluding shadowed or snowy image pixels. Next, we computed the average value of the ratio between Autumn/Winter NDVI and Spring/Summer NDVI for each land-cover class. Finally, we reconstructed a synthetic pixel-based map for Autumn/Winter NDVI by multiplying the Spring/Summer NDVI by the average ratio computed at the previous step, for each land-cover class.

Once the time series of NDVI were reconstructed, we estimated the C-factor time series. For each land-cover class of DUSAF we defined a range of possible values for C-factor $[C_{n,min}, C_{n,max}]$, based on past studies (see Table 1 and Gianinetto et al., 2018) and then linearized C-factor with NDVI as follows:

where:

$$C_n = \begin{cases} C_{n,max} \text{ FOR } NDVI < NDVI_{n,min} \\ C_{n,max} + \frac{NDVI - NDVI_{n,min}}{NDVI_{n,max} - NDVI_{n,min}} \left(C_{n,min} - C_{n,max}\right) \text{ FOR } NDVI_{n,min} \le NDVI \le NDVI_{n,max} \\ C_{n,min} \text{ FOR } NDVI > NDVI_{n,max} \end{cases} \tag{13}$$

$C_{n,min}$ [-] is the minimum C-factor value for land-cover class n;

$C_{n,max}$ [-] is the maximum C-factor value for land-cover class n;

$NDVI_{n,min}$ [-] is a threshold for land-cover class n set to $\mu_{NDVI} - \sigma_{NDVI}$;

OM [-] is a threshold for land-cover class n set to $\mu_{NDVI} + \sigma_{NDVI}$.

To guarantee time and space coherence of seasonal C-factor estimates, we use the same thresholds for both Spring/Summer and Autumn/Winter images. Pixel corresponding to non-vegetated classes in DUSAF were assigned a null C-factor (Figure 8(e)).

Results

Figure 9 compares the estimates of potential soil erosion rates simulated with D-RUSLE (SIM_07) and RUSLE (SIM_01). D-RUSLE takes into account a regional-based mapping of the parameters, snow cover dynamics and both inter-annual and intra-annual variability of land cover as follows:

- Rainfall erosivity is modelled using the R2 parametrization, as it separates rainfall and snow contribution to soil erosion, thus providing seasonal and altitude discrimination which are important in the mountainous environment;

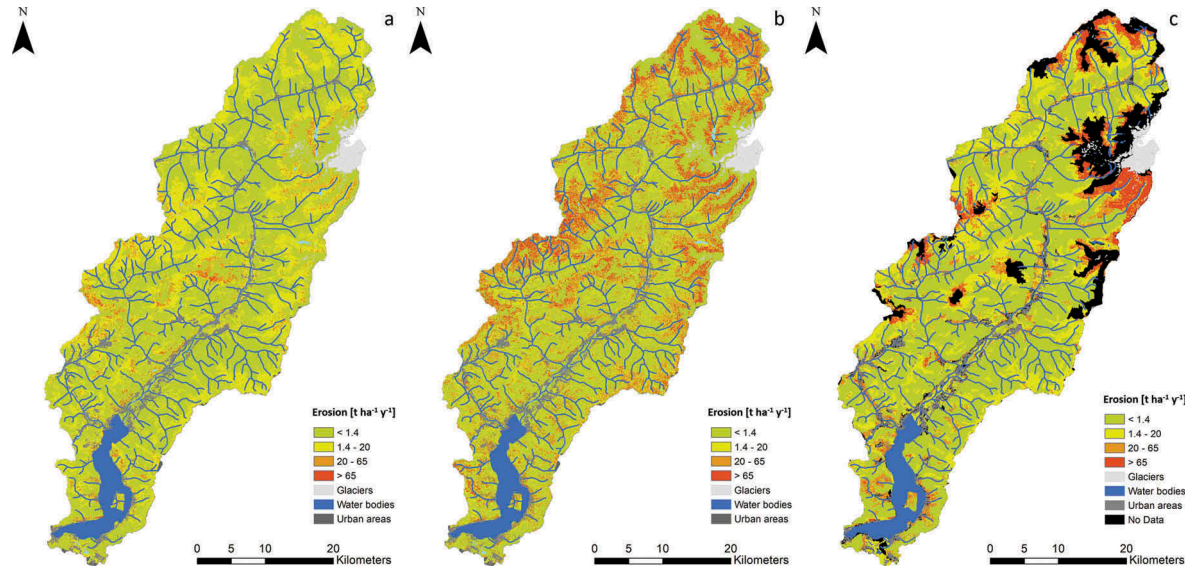

Figure 9. Comparison of potential soil erosion maps simulated with: (a) D-RUSLE (SIM_07), (b) classic RUSLE (SIM_01) and c) JRC RUSLE.

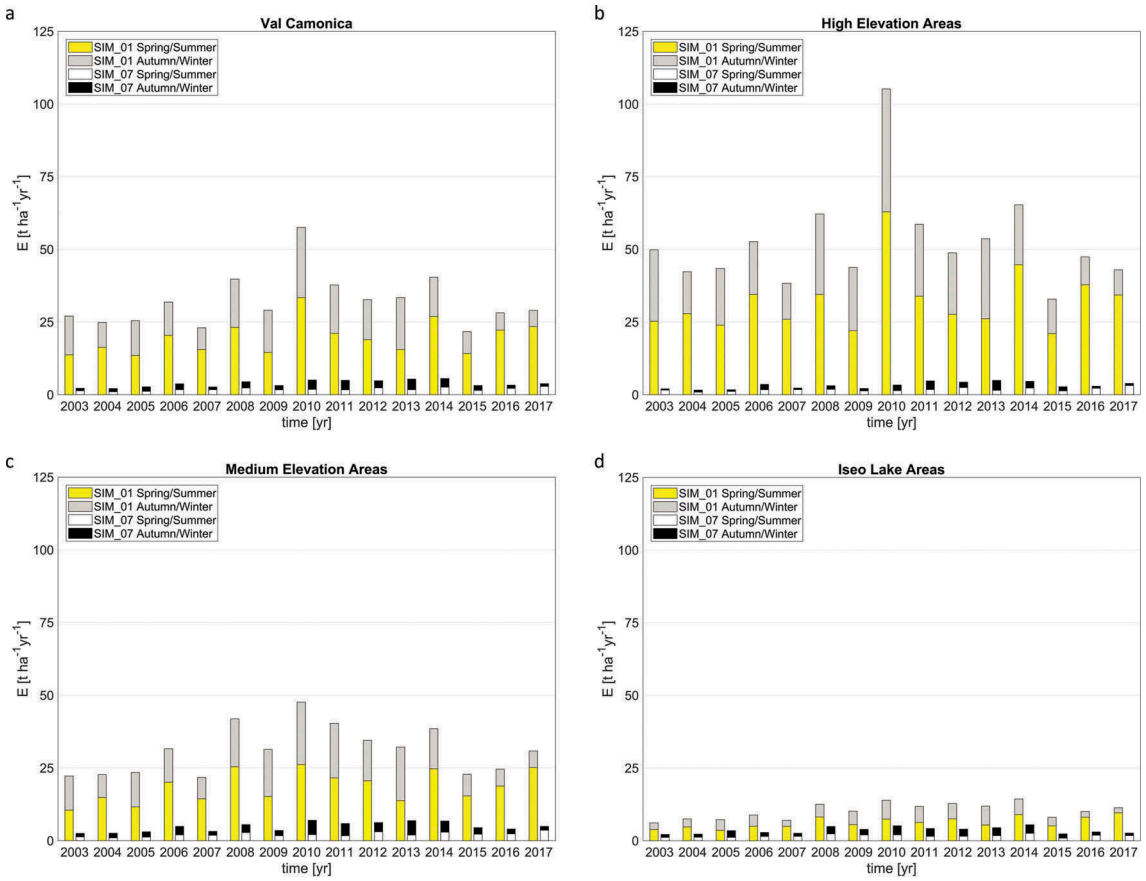

Figure 10. Comparison of potential soil erosion rates (2003–2017) computed for Spring/Summer and Autumn/Winter with D-RUSLE (SIM_07) and classic RUSLE (SIM_01).

- Soil erodibility is modelled using the K2 parametrization, as it can be applied to other case studies;
- Slope length and steepness are modelled using the LS2 parametrization, as suggested by reference works in the literature;
- Cover management type is modelled using the C2 parametrization, as satellite images can greatly improve the dynamic estimation of the sheltering effect of vegetation;
- Conservation practice is neglected in the absence of field information.

Although the two approaches provide a different range of erosion rates variability, due to different parameters' formulation, their spatial patterns can be compared. That is showed in Figure 9: overall, higher erosion areas are predominantly located at higher altitudes on slopes, while lower erosion values characterize valley areas. Nevertheless, the adoption of D-RUSLE (Figure 9(a)) leads to a decrease in soil loss estimates, more than eight-fold with respect to the classic RUSLE (Figure 9(b)), with a larger difference in the high elevation areas. This difference decreases to a fifth in the lake area (Figure 10).

Benchmark

The potential soil loss rate is a difficult quantity to measure in the field; thus, we used the most recent reference data available for Europe (Panagos et al., 2015a) as a benchmark (Figure 9(c)).

The comparison between JRC erosion estimates on Val Camonica area and D-RUSLE (SIM_07) estimates shows a general agreement on the location of the areas more prone to erosion, given the different spatial resolution of the studies: 100-m (aggregated) for JRC output (Panagos et al., 2015a) and 30-m for our results (Aiello et al., 2018a). No data values (almost 16% of the study area) in JRC map are due to a lack of data in the C-factor estimate (Panagos et al., 2015b).

Comparison with plot scale erosion experiments

One of the main limitations for ground truth validation of RUSLE-like models, including D-RUSLE, is that the models do not include a sediment transport and deposition module and they are not aimed to simulate single events. Thus, they are expected to provide potential yearly erosion rates, while usually available measurements refer to net erosion rates. Moreover, it has to be considered that in-situ observations are often characterized by considerable uncertainties, due to the highly heterogeneous nature of soil erosion and the tendency of erosion measurements of being very prone to errors (Alewell, Borelli, Meusburger, & Panagos, 2019). Nevertheless, in July 2017, we made two field experiments to evaluate soil erosion at a local scale (for similar experiments and technical details see Rulli, Bozzi, Spada, Bocchiola, & Rosso, 2006). The test site was *Case di Viso* (Figure 5), located in the Northern part of the catchment at an altitude of 1900 [m a.s.l.], selected because paradigmatic of the alpine vegetation cover in the study area and also easily accessible.

Two experiments were carried out on a grassland plot covering an area of about 144 [m^2], for undisturbed (dry) initial soil moisture condition (experiment nr. 1), and wet soil (experiment nr. 2). Using a rainfall simulator, rainfall events of high intensity and short duration were generated to produce a measurable erosion at the plot scale. A rainfall intensity of 70 mmh^{-1} was generated, corresponding to ca. 200 years return period according to intensity-duration-frequency curves available from the Environmental Protection Agency of Regione Lombardia, for 18 min (experiment nr. 1) and 30 min (experiment nr. 2). The runoff (liquid and solid) were collected during the experiment, and suspended sediment and particle size analysis were carried out ex-post.

The experimental plot approximatively corresponds to only 1/6 of the Landsat pixel. However, being representative of the surrounding landscape and land cover, results can be extended to the whole corresponding satellite image pixel. The field experiments returned the net erosion but the D-RUSLE modelling simulated the potential erosion; therefore, we applied an inflow coefficient for the comparison of results as proposed by Yang (1972, 1973). Particles smaller than 0.0288 mm (*D50*, i.e. the diameter at which 50% of the sample's mass is comprised of particles with a diameter less than this value) were used as representative of the sediment's diameter during the initial part of the experiment, as proposed by Shi et al. (2012). However, as soon as the runoff increased, *D60* (i.e. the diameter at which 60% of the sample's mass is comprised of particles with a diameter less than this value, *D60* is equal to 0.106 mm in our case) were used. That because the smaller particles are usually eroded immediately and the larger particles start being eroded as soon as smaller ones become rarer.

So doing, we were able to reproduce the trend of sediment transport with acceptable accuracy. The comparison of the D-RUSLE modelling with the observed sediments led to an accuracy of 11.7% (the cumulative sediment was 3229 [mg] while the model returns a net erosion of 3608 [mg]) for initial dry condition and shorter rainfall duration (experiment nr.1) and 33.1% (the cumulative sediment was 11,001 [mg] while the model simulates 14,644 [mg]) for initial wet condition and longer rainfall duration (experiment nr. 2). These results suggest that results obtained with the D-RUSLE approach are reasonable, even if the field experiments and the D-RUSLE analysis are carried out at a very different scale.

Sensitivity analysis

Several simulations are used to evaluate the models' sensitivities to the different parametrization of input variables (Table 3). Therein, simulation code SIM_01 corresponds to classic RUSLE, here used as a reference,

Table 3. Different combinations of the parameters.

	Parameters' code			
Simulation code	R-factor	C-factor	K-factor	LS-factor
SIM_01	R1	C0	K1	LS1
SIM_02	R2	C0	K1	LS1
SIM_03	R1	C0	K2	LS1
SIM_04	R1	C0	K1	LS2
SIM_05	R1	C1	K1	LS1
SIM_06	R1	C2	K1	LS1
SIM_07	R2	C2	K2	LS2

while simulation code SIM_07 corresponds to the D-RUSLE model here proposed. Intermediate simulations (from SIM_02 to SIM_06) show the impact on the estimate of different input variables parametrization.

Sensitivity to R-factor

On average, the R2 parametrization produces lower rainfall erosivity compared to the R1 parametrization (μ_{R1}= 1094 [MJ mm ha^{-1}h^{-1}yr^{-1}], μ_{R2}= 439 [MJ mm ha^{-1}h^{-1}yr^{-1}]), with almost comparable dispersion (σ_{R1}= 141 [MJ mm ha^{-1}h^{-1}yr^{-1}], σ_{R2}= 163 [MJ mm ha^{-1}h^{-1}yr^{-1}]). In particular, the R1 parametrization overestimates rainfall erosivity in Autumn/Winter, as it does not distinguish between snow and rainfall and does not account for snow cover.

Consequently, using the R2 parametrization (SIM_02) instead of the standard R1 (SIM_01) produces lower potential soil erosion rates. The most significant decrease is located in high and medium elevation areas, where soil loss rates decrease of 75% and 63%, respectively, due to the modelling of snowfall and snow cover dynamics. A minor decrease (47%) is estimated in the lake areas, as a result of lower altitudes that limit snowfall occurrence and accelerates snow melting process. Overall, using R2 instead of R1 had the highest impact on simulations (−68% of potential soil erosion rates).

Sensitivity analysis respect to K-factor

The effect of using K2 parametrization (SIM_03) instead of the more complex and detailed K1 parametrization (SIM_01) is not uniform within the study area. Overall, K2 parametrization produces a lower spatial variability, as each polygon of the reference soil map is assigned a single value (Figure 8(b)). Nevertheless, statistics are comparable (μ_{K1}= 0.0228 [t ha h ha^{-1}MJ^{-1}mm^{-1}], μ_{K2}= 0.0236 [t ha h ha^{-1}MJ^{-1}mm^{-1}], σ_{K1}= 0.0097 [t ha h ha^{-1}MJ^{-1}mm^{-1}], σ_{K2}= 0.0112 [t ha h ha^{-1}MJ^{-1}mm^{-1}]).

More in detail, the use of K2 parametrization has a mixed impact: potential soil loss rate decreases by almost 50% in high elevation areas, while it increases by almost 60% in the Iseo Lake area. The impact of K2 parametrization is limited in medium elevation areas (−16%). Therefore, moving from K1 to K2 parametrization the overall potential erosion rate decreases by 27%. This reflects the different spatial distribution of K-factor using K1 and K2 parametrizations, as shown in Figures 6(b), 8(b).

Sensitivity analysis with respect to LS-factor

LS2 parametrization (SIM_04) is very different from the classic LS1 parametrization (SIM_01), both in terms of mean (μ_{LS1}= 29.6, μ_{LS2}= 13.0) and standard deviation (σ_{LS1}= 38.7, σ_{LS2}= 15.0). However, past studies suggested that LS2 is to be preferred for sub-basin scale analysis (Panagos, Borrelli, & Meusburger, 2015).

The adoption of LS2 parametrization has an important impact on the modelling, with an overall decrease of potential soil erosion rate of about 55%, regardless of the elevation ranges.

Sensitivity analysis with respect to C-factor

Simulation SIM_06 (C2) returns slightly increasing rates with respect to SIM_01 (C0). Nevertheless, values are almost comparable among all the three altitude areas (+19%, +13% and −6% for SIM_06 in high altitude, in medium altitude and in lake areas, respectively), as all both approaches rely on the use of land-cover classes to limit C-factor variability. On the contrary, simulation SIM_05 (C1) returns a prominent increase (nearly three times) in soil loss rates estimates, due to no boundaries that limit the variability of C-factor estimates. This effect is particularly evident in the lake area (+296%), characterized by a predominance of forests, and slightly decreases when moving to higher altitudes (+188% for medium elevation area and +127% for high elevation area), where forests are replaced by sparsely vegetated areas.

On the whole area, the use of C2 parametrization showed a limited effect of average soil erosion rates (+12%), but differences between C0 and C2 parametrization are evident when data are analysed at seasonal scale as in Section 6.2.

Discussion

Correlation between model's parameters and soil erosion estimates

The sensitivity analysis points out that the parametrization of R-factor has the highest impact on the average potential soil erosion, when not considering the simulation SIM_05 that is biased by

Table 4. Pearson's correlation between modelling parameters and erosion maps.

	Parameters			
Simulation code	R-factor	C-factor	K-factor	LS-factor
SIM_01	0.03	0.54	0.22	0.29
SIM_02	−0.08	0.53	0.19	0.29
SIM_03	0.04	0.52	0.02	0.29
SIM_04	0.04	0.69	0.27	0.19
SIM_05	0.04	0.54	0.25	0.44
SIM_06	0.02	0.59	0.23	0.29
SIM_07	0.02	0.51	0.08	0.20

the C-factor overestimation. However, a pixel-based Pearson's correlation with the erosion maps shows that the R-factor is always an uncorrelated variable, regardless of the parametrization used (Table 4).

On the other hand, while the C-factor (SIM_06 vs SIM_01) has the lowest impact on soil erosion rates, this parameter is still the most correlated with the erosion maps, regardless of the parametrization used (Table 4). Even if the different parametrization of K-factor is characterized by comparable statistics, their different spatial variability (K2 is more homogenous than K1) strongly reduces the correlation between K-factor and expected erosion rate, SIM_03 and SIM_07, using K2 formulation, show the lowest correlation coefficient with K-factor.

The impact of LS-factor parametrization on the average soil erosion rates is about −56% (SIM_04 vs SIM_01), which is comparable with an average reduction of LS-factor retrieved passing from LS1 to LS2, and the correlation coefficient consequently reduces from 0.29 (SIM_01) to 0.19 (SIM_04).

Effect of seasonality on soil erosion estimates

Precipitation regime (i.e. R-factor) and land-cover variability (i.e. C-factor) are the parameters that convey seasonality in D-RUSLE. Simulations SIM_02, SIM_05 and SIM_06 show this effect (Table 5).

SIM_02 retrieves lower soil erosion rates, as a consequence of introducing snow dynamics and the protective effect of snow cover. SIM_05 and

Table 5. Average Spring/Summer (S/S) and Autumn/Winter (A/W) erosion estimates.

	Val Camonica [t ha^{-1} yr^{-1}]		High Elevation Areas [t ha^{-1} yr^{-1}]		Medium Elevation Areas [t ha^{-1} yr^{-1}]		Iseo Lake Areas [t ha^{-1} yr^{-1}]	
Season	S/S	A/W	S/S	A/W	S/S	A/W	S/S	A/W
SIM_01	19.54	12.58	32.19	20.31	18.58	12.53	6.31	3.96
SIM_02	6.91	3.24	9.32	3.89	7.64	3.79	3.47	1.96
SIM_05	17.35	66.95	27.59	91.22	14.20	75.74	8.96	31.04
SIM_06	15.95	20.15	28.53	32.37	13.45	21.25	4.30	5.37

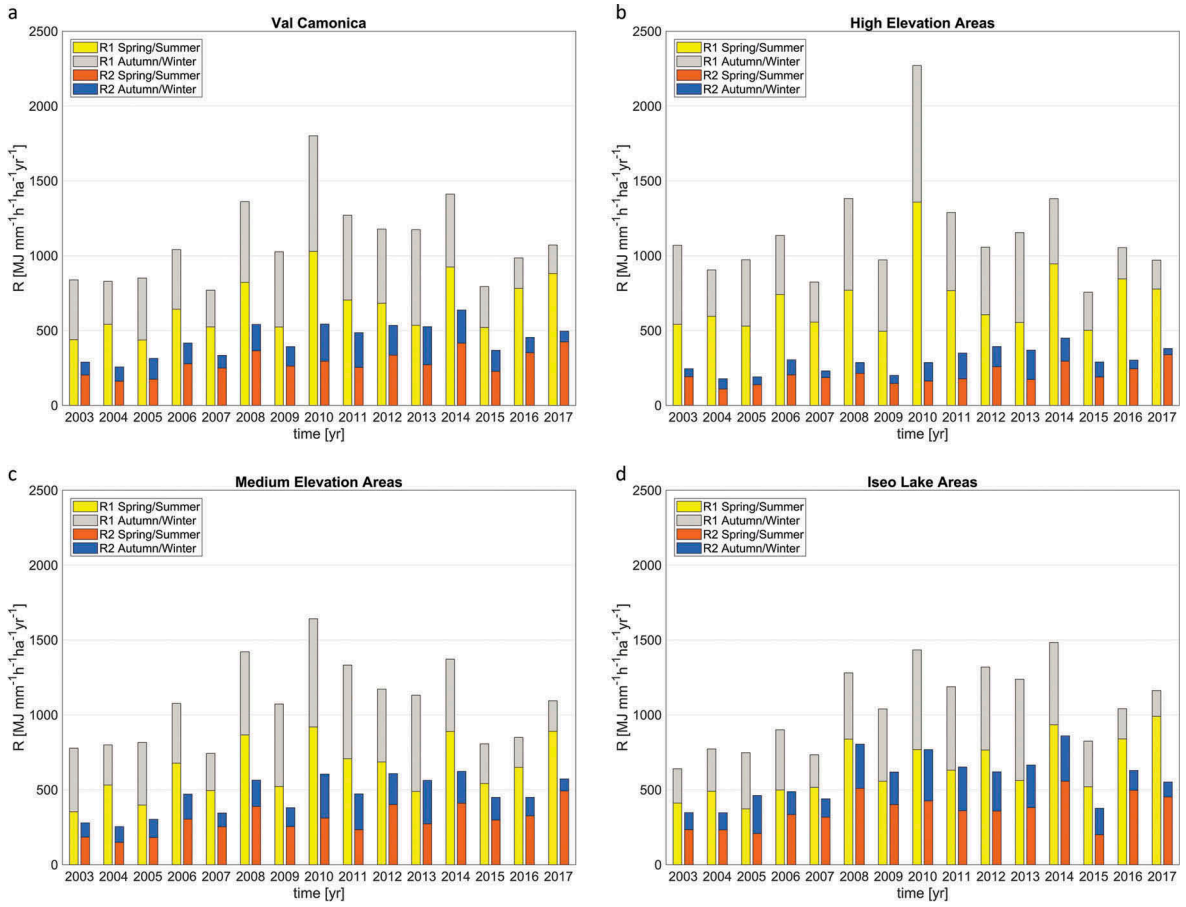

Figure 11. Time series of R-factor (2003–2017) computed for Spring/Summer and Autumn/Winter with the R1 (SIM_01) and R2 (SIM_02) parametrizations.

SIM_06 introduce a dynamic estimate of C-factor, which translates into a smaller sheltering effect of vegetation during Autumn/Winter. This increases Autumn/Winter erosion estimates, leading to higher erosion rates in Autumn/Winter with respect to Spring/Summer. It is to be noted that traditional RUSLE does not model this dynamic and the modelled Autumn/Winter erosion rates are smaller than Spring/Summer erosion estimates (SIM_01). However, that is not consistent with the phenology of vegetation cover.

The out-of-range Autumn/Winter erosion values of SIM_05 are due to the underestimated protective effect of vegetation (C1 parametrization), particularly for forest areas, which leads to an overestimation of soil erosion rates (see Section 4.2).

Table 5. Average Spring/Summer (S/S) and Autumn/Winter (A/W) erosion estimates.

Figure 11 shows the comparison of the R-factor time series for Spring/Summer and Autumn/Winter. The seasonal effect is much more clearly highlighted by the R2 parametrization, as it explicitly separates snowfall and rainfall and considers the soil sheltered by snow cover. Thus, Spring/Summer erosive force exceeds Autumn/Winter erosive force, because Spring/Summer rainfall is more abundant and almost no snow cover is present. The effect of seasonality when using the R2 parametrization (SIM_02) is to decrease potential soil erosion rates of almost 3 times during Spring/Summer and 4 times during Autumn/Winter, compared to the classic parametrization (SIM_01) (Table 5 and Figure 12). This reduction is much more evident in the high altitude areas and it decreases moving towards the lake area, where lower erosion rates are seen.

Figure 13 shows the comparison of the C-factor time series for Spring/Summer and Autumn/Winter. The reduced vegetation abundance in Autumn/Winter produces higher values for both C1 and C2 parametrizations, while this is not accounted for by the "static" C0 parametrization. Slightly higher cover management factor values are estimated in the high altitude areas, due to the presence of sparsely vegetated areas and moors. On the other hand, the Iseo Lake area has the opposite behaviour because of the presence of a larger vegetation cover protecting the soil from erosion. As already mentioned in Section 4.2, C-factor is overestimated when using unbounded relationships with NDVI (C1).

Consequently, estimates of potential soil erosion rates reflect the seasonality effect given by land cover. However, in simulation SIM_01 only the effect of

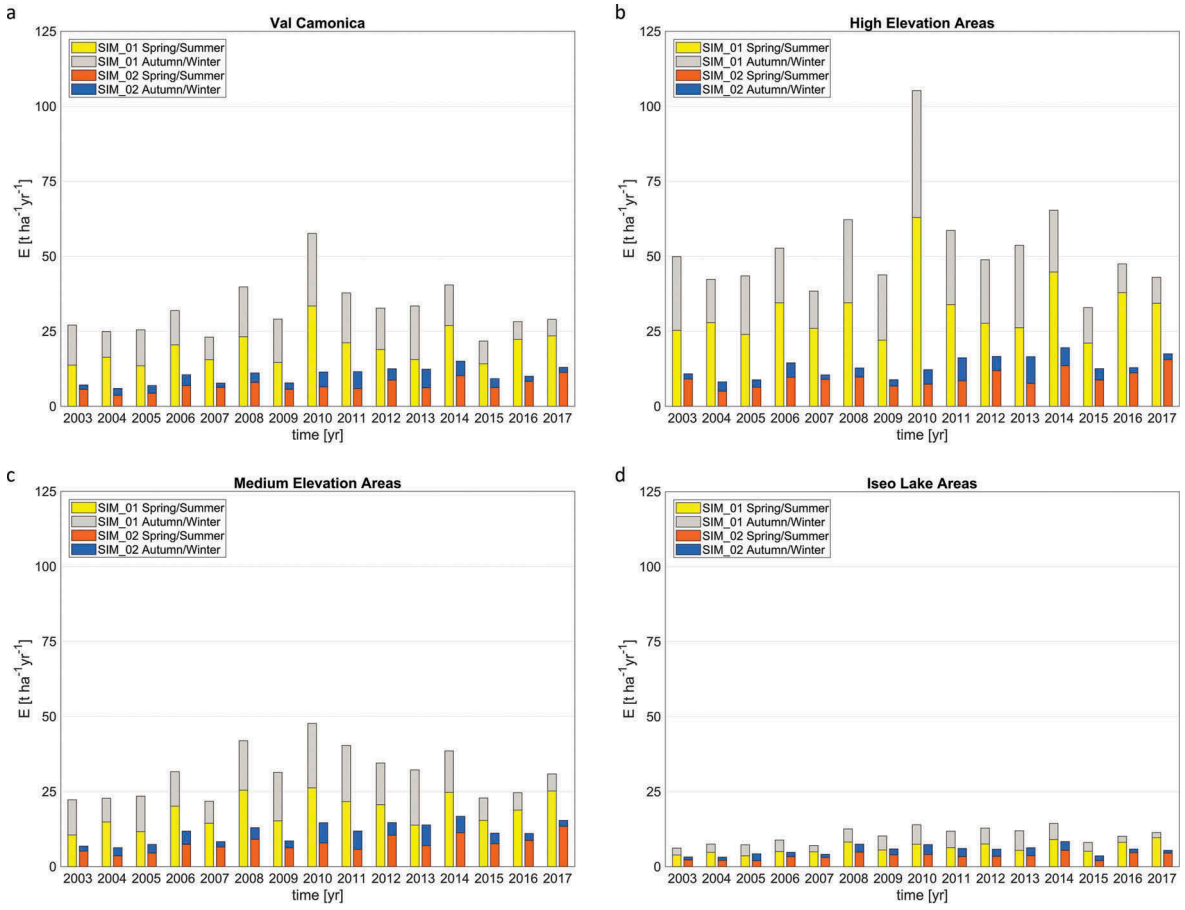

Figure 12. Comparison of potential soil erosion rates (2003–2017) computed for Spring/Summer and Autumn/Winter with the R1 (SIM_01) and R2 (SIM_02) parametrizations.

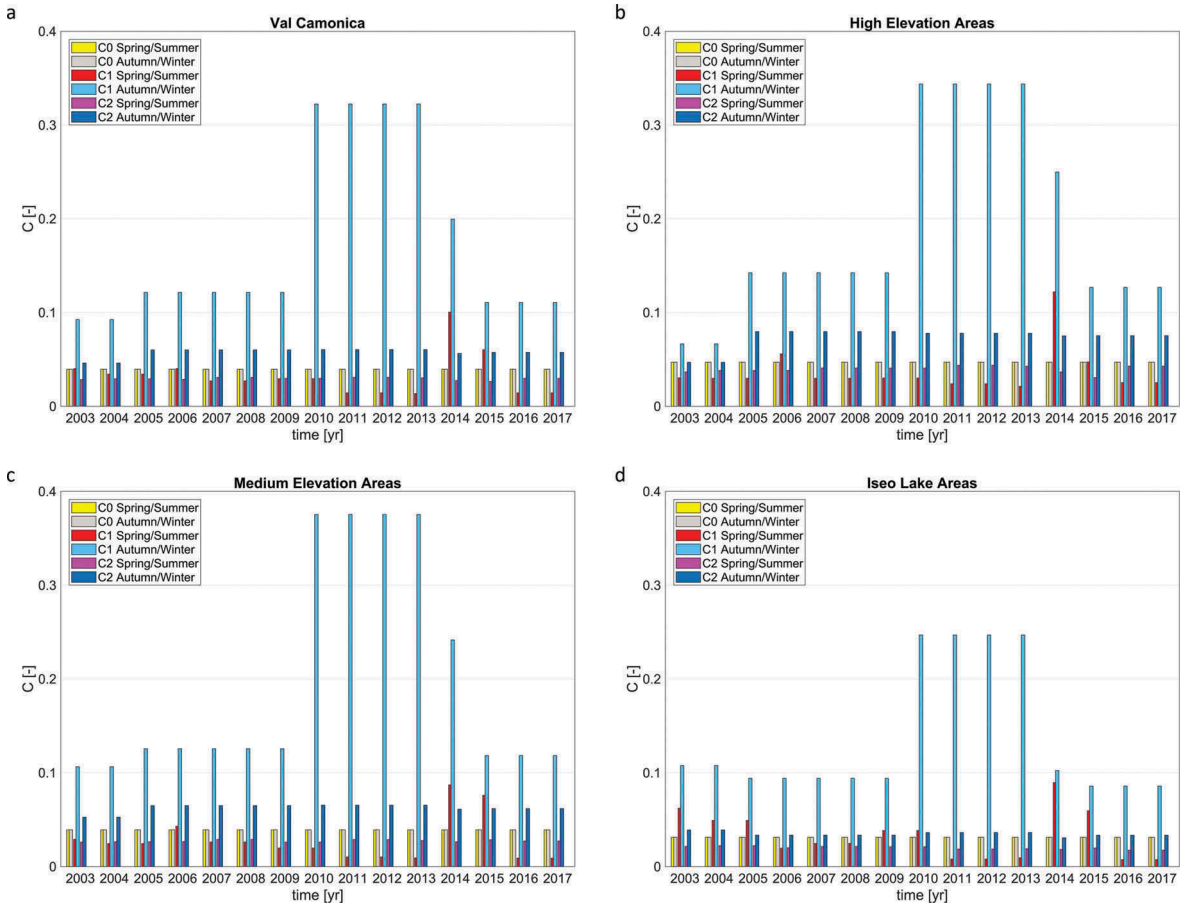

Figure 13. Time series of C-factor (2003–2017) computed for Spring/Summer and Autumn/Winter with the C0 (SIM_01), C1 (SIM_05) and C2 (SIM_06) parametrizations.

precipitation seasonality is present, as the C0 cover management factor parametrization is constant over time.

In simulations SIM_05 and SIM_06, the seasonality effect comes from both land-cover changes and rainfall/snow seasonality. Spring/Summer erosion estimates with the parametrization of SIM_06 are slightly lower with respect to those simulated with the parametrization of SIM_05, as a consequence of the bounding on C values. In contrast, during Autumn/Winter, erosion rates of SIM_05 are overestimated because of low NDVI values causing overestimates of C-factor, exceeding the SIM_05 estimates by almost four times (Table 5).

The use of multi-temporal satellite time series for the computation of C-factor (SIM_06 simulation) produces a slight increase in Autumn/Winter erosion estimates and a slight decrease in Spring/Summer ones (Figure 14). Besides, the estimates of soil loss rates decrease from high altitude to the lake area, meaning that during Autumn/Winter land-cover types have a higher influence on erosion modelling compared to rainfall.

Overall, the computation of the model's parameters for the Autumn/Winter season seems the most critical for soil erosion in the Italian Alps.

Issues and possible improvements

If land-cover maps are not available, the C1 parametrization provides an estimate of the cover management factor, although it overestimates soil erosion for forest areas and Autumn/Winter season (Section 4.2). Thus, this parametrization could be further improved by tuning the coefficients of Equation (12) to avoid unreliable erosion estimates. However, specific experimentation is needed at the local scale.

Moreover, optical images cannot be collected in cloudy weather, and images taken in shadowed areas are often useless. This is a well-known limitation of multispectral Remote Sensing in mountain areas and typically occurring during the Winter. On the other hand, satellite imagery could complement the modelling of snow dynamics providing maps of snow cover, that could be enhanced by extending the Landsat surveys with Sentinel-2 images. This may also have further effect of improving the mapping spatial detail.

D-RUSLE could also be further improved by estimating different sets of input parameters for each season (Winter, Spring, Summer and Autumn), thus extending the seasonal dynamics here introduced as two macro-seasons (Autumn/Winter and Spring/Summer).

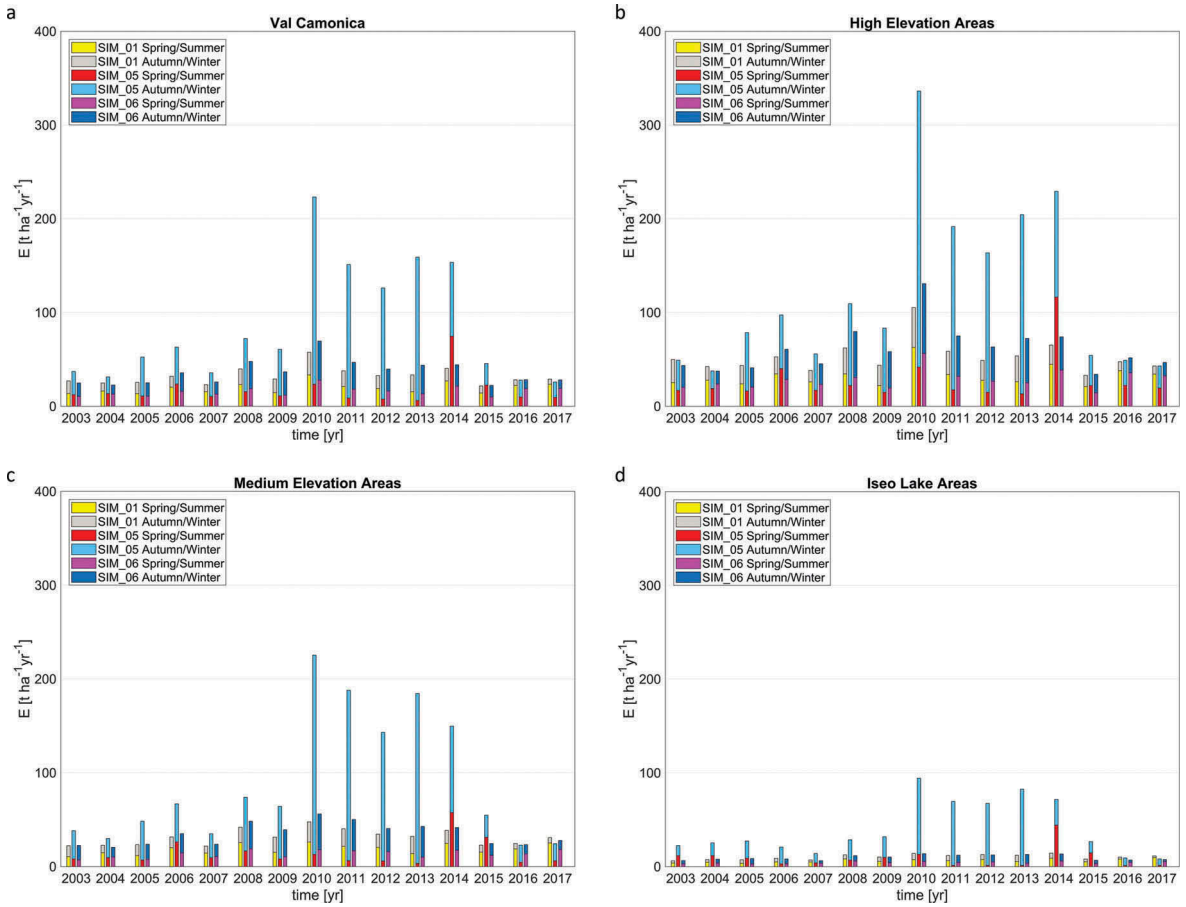

Figure 14. Comparison of potential soil erosion rates (2003–2017) computed for Spring/Summer and Autumn/Winter with the C0 (SIM_01), C1 (SIM_05) and C2 (SIM_06) parametrizations.

Finally, D-RUSLE could be further refined by introducing a parametrization for the support practice (P-factor). Likely, however, this improvement would have an impact mainly on terraced agricultural areas.

The results of our plot scale experiment, briefly reported above are of some interest. Indeed, in spite of the considerable difference in scale, and complexity of erosion phenomena, such preliminary results seemingly indicate that the approach provided here may depict reasonably distributed soil erosion within the catchment. Further plot scale experiments may be pursued for spatially distributed validation of the model, also considering seasonal variations.

Conclusions

Recently, many environmental protection agencies have recognized soil degradation due to erosion processes as a serious threat, and the European Commission addresses soil degradation as a key priority within its Soil Thematic Strategy. Therefore, soil erosion models are extremely useful for quantifying the impact of soil loss at the basin scale, assessing the potential effects of climate-driven land-cover changes on soil erosion rates, defining priorities for effective and sustainable land management actions (i.e. re-vegetation of sparsely vegetated areas with high soil loss rates).

In this work, we proposed a RUSLE-like dynamic model (D-RUSLE) to estimate potential soil erosion rates and we tested its performances in the fragile ecosystem of the Italian Alps, where climate change, together with both natural and anthropogenic land transformations, contribute to soil degradation.

With respect to the classic RUSLE, (i) the exploitation of satellite images allow simulating the intra- and inter-annual variability of land use and land-cover parameter, highlighting rainfall erosivity and vegetation cover as limiting factors to soil erosion during Autumn/Winter and Spring/Summer, respectively; (ii) rainfall erosivity estimate takes into account snow dynamics and (iii) similar seasonal soil erosion rates are mainly related to opposite dynamics of rainfall erosivity and land use/land cover.

Therefore, the main contribution of this work is to integrate the RUSLE model with optical satellite images both directly, for the estimate of the land-cover factor through the NDVI, and indirectly, for validating the snow accumulation and melting model used for rainfall erosivity estimation.

Our model is able to catch variations in potential soil erosion due to different landscape characteristics:

higher rates were found within the land-cover classes which are more affected by seasonality (e.g. broad-leaved forests), alike higher altitude areas which were more prone to erosion due to sparse or absent vegetation coverage, while forested areas at lower altitudes were found less exposed to erosion. Moreover, D-RUSLE showed that integrating satellite-derived information in the estimation of C-factor helps in providing a more detailed and reliable estimate of potential soil loss, both including seasonal and long-term land-cover changes. In particular, the use of satellite images may increase the spatial resolution of C-factor improving the estimates of soil erosion at regional/local scale, in particular in areas where vegetation is the predominant land cover. Besides, Spring/Summer and Autumn/Winter contribution to soil erosion can be evaluated separately and focused actions towards soil erosion could be pursued.

Acknowledgements

The Authors kindly acknowledge: (i) Parco dell'Adamello and Comunità Montana della Val Camonica for their support and interest in the project and for supplying useful data; (ii) Regione Lombardia-Regional Territorial Office (Brescia) for information and data on the study area; (iii) ENEL Production for data on sediment deposition rates within their dams, and (iv) Servizio Glaciologico Lombardo for their help and Dept. ESP of University Milano for their support in modelling of glaciers' coverage in the Adamello area.

Disclosure statement

No potential conflict of interest was reported by the authors.

Funding

This work was supported by Fondazione Cariplo, which funded the research project Hydrogeological modeling for Erosion Risk Assessment from SpacE (HERASE) for the years 2017-2019 (Grant Nr. 2016-0768).

ORCID

Giovanni Ravazzani http://orcid.org/0000-0002-6850-0883
Andrea Soncini http://orcid.org/0000-0001-9011-616X

References

Aiello, A., Adamo, M., & Canora, F. (2015). Remote sensing and GIS to assess soil erosion with RUSLE3D and USPED at river basin scale in southern Italy. *Catena*, *131*, 174–185. doi:10.1016/j.catena.2015.04.003

Aiello, M., Gianinetto, M., Vezzoli, R., Rota Nodari, F., Polinelli, F., Frassy, F., … Bocchiola, D. (2018a). Modelling soil erosion in the Alps with dynamic RUSLE-like model and satellite observations. *Proceedings of the Italian Society of Remote Sensing conference 2018*. Florence, Italy.

Aiello, M., Vezzoli, R., Polinelli, F., Frassy, F., Rota Nodari, F., Rulli, M.C., … Gianinetto, M., (2018b, November). Analisi di sensitività nella stima dell'erosione di suolo nelle Alpi con misure in situ e serie temporali Landsat. *Acts of the XXII Conferenza Nazionale ASITA 2018*. Bolzan, Italy.

Alewell, C., Borelli, P., Meusburger, K., & Panagos, P. (2019). Using the USLE: Chances, challenges and limitations of soil erosion modelling. *International Soil and Water Conservation Research*. doi:10.1016/j.iswcr.2019.05.004

Beasley, D.B., Huggins, L.F., & Monke, A. (1980). ANSWERS: A model for watershed planning. *Transactions of the ASAE*, *23*(4), 938–0944. doi:10.13031/2013.34692

Beskow, S., Mello, C.R., Norton, L.D., Curi, N., Viola, M.R., & Avanzi, J.C. (2009). Soil erosion prediction in the Grande River Basin, Brazil using distributed modeling. *Catena*, *79*(1), 49–59. doi:10.1016/j.catena.2009.05.010

Bosco, C., Rusco, E., Montanarella, L., & Panagos, P. (2009). Soil erosion in the Alpine area: Risk assessment and climate change. *Studi Trentini Di Scienze Naturali*, *85*, 117–123.

COM. (2006). *231 final communication from the commission to the council, the European parliament, the European economic and social committee and the committee of the regions*. Thematic Strategy for Soil Protection (2006).

Desmet, P.J.J., & Govers, G. (1996). A GIS procedure for automatically calculating the USLE LS factor on topographically complex landscape units. *Journal of Soil and Water Conservation*, *51*(5), 427–433.

Fantappiè, M., Priori, S., & Costantini, E.A.C. (2015). Soil erosion risk, Sicilian region (1: 250,000 scale). *Journal of Maps*, *11*(2), 323–341. doi:10.1080/17445647.2014.956349

Feoli, E., Vuerich, L.G., & Zerihun, W. (2002). Evaluation of environmental degradation in northern Ethiopia using GIS to integrate vegetation, geomorphological, erosion and socio-economic factors. *Agriculture, Ecosystems & Environment*, *91*(1–3), 313–325. doi:10.1016/S0167-8809(01)00236-5

Fernandez, C., Wu, J.Q., McCool, D.K., & Stöckle, C.O. (2003). Estimating water erosion and sediment yield with GIS, RUSLE, and SEDD. *Journal of Soil and Water Conservation*, *58*(3), 128–136.

Ferro, V., & Porto, P. (2000). Sediment delivery distributed (SEDD) model. *Journal of Hydrologic Engineering*, *5*(4), 411–422. doi:10.1061/(ASCE)1084-0699(2000)5:4(411)

Flügel, W.A., Märker, M., Moretti, S., Rodolfi, G., & Sidrochuk, A. (2003). Integrating geographical information systems, remote sensing, ground truthing and modelling approaches for regional erosion classification of semi-arid catchments in South Africa. *Hydrological Processes*, *17*(5), 929–942. doi:10.1002/hyp.1171

Gianinetto, M., Aiello, M., Vezzoli, R., Rota Nodari, F., Polinelli, F., Frassy, F., … Corbari, C. (2018, September). Satellite-based cover management factor assessment for soil water erosion in the Alps. *Proceedings of the Remote Sensing for Agriculture, Ecosystems, and Hydrology XX* (Vol. 10783, p. 107830T). International Society for Optics and Photonics. Berlin, Germany.

Igwe, P.U., Onuigbo, A.A., Chinedu, O.C., Ezeaku, I.I., & Muoneke, M.M. (2017). Soil erosion: A review of models and applications. *International Journal of Advanced Engineering Research and Science*, *4*(12), 138-150.

Knisel, W.G. (1980). CREAMS: A field scale model for chemicals, runoff, and erosion from agricultural management systems [USA]. *United States. Dept. of Agriculture. Conservation research report (USA)*.

Laflen, J.M., Lane, L.J., & Foster, G.R. (1991). WEPP: A new generation of erosion prediction technology. *Journal of Soil and Water Conservation*, *46*(1), 34–38.

Merritt, W.S., Letcher, R.A., & Jakeman, A.J. (2003). A review of erosion and sediment transport models. *Environmental Modelling & Software*, *18*(8–9), 761–799. doi:10.1016/S1364-8152(03)00078-1

Mitasova, H., Hofierka, J., Zlocha, M., & Iverson, L.R. (1996). Modelling topographic potential for erosion and deposition using GIS. *International Journal of Geographical Information Systems*, *10*(5), 629–641. doi:10.1080/02693799608902101

Morgan, R.P.C., Quinton, J.N., Smith, R.E., Govers, G., Poesen, J.W.A., Auerswald, K., … Styczen, M.E. (1998). The european soil erosion model (EUROSEM): A dynamic approach for predicting sediment transport from fields and small catchments. *Earth Surface Processes and Landforms: the Journal of the British Geomorphological Group*, *23*(6), 527–544. doi:10.1002/(ISSN)1096-9837

Panagos, P., Borrelli, P., & Meusburger, K. (2015). A new European slope length and steepness factor (LS-Factor) for modeling soil erosion by water. *Geosciences*, *5*(2), 117–126. doi:10.3390/geosciences5020117

Panagos, P., Borrelli, P., Meusburger, K., Alewell, C., Lugato, E., & Montanarella, L. (2015b). Estimating the soil erosion cover-management factor at the European scale. *Land Use Policy*, *48*, 38–50. doi:10.1016/j.landusepol.2015.05.021

Panagos, P., Borrelli, P., Poesen, J., Ballabio, C., Lugato, E., Meusburger, K., … Alewell, C. (2015a). The new assessment of soil loss by water erosion in Europe. *Environmental Science & Policy*, *54*, 438–447. doi:10.1016/j.envsci.2015.08.012

Panagos, P., Meusburger, K., Ballabio, C., Borrelli, P., & Alewell, C. (2014). Soil erodibility in Europe: A high-resolution dataset based on LUCAS. *Science of the Total Environment*, *479*, 189–200. doi:10.1016/j.scitotenv.2014.02.010

Renard, K.G., Foster, G.R., Weesies, G.A., McCool, D.K., & Yoder, D.C. (1997). *Predicting soil erosion by water: A guide to conservation planning with the Revised Universal Soil Loss Equation (RUSLE)* (Vol. 703). Washington, DC: United States Department of Agriculture.

Rosso, R., Rulli, M.C., & Bocchiola, D. (2007). Transient catchment hydrology after wildfires in a Mediterranean basin: Runoff, sediment and woody debris. *Hydrology and Earth System Sciences*, *11*, 125–140. doi:10.5194/hess-11-125-2007

Rulli, M.C., Bozzi, S., Spada, M., Bocchiola, D., & Rosso, R. (2006). Rainfall simulations on a fire disturbed mediterranean area. *Journal of Hydrology*, *327*(3–4), 323–328. doi:10.1016/j.jhydrol.2005.11.037

Rulli, M.C., Offeddu, L., & Santini, M. (2013). Modeling post-fire water erosion mitigation strategies. *Hydrology and Earth System Science*, *17*(6), 2323–2337. doi:10.5194/hess-17-2323-2013

Rulli, M.C., & Rosso, R. (2005). Modeling catchment erosion after wildfires in the San Gabriel Mountains of southern California. *Geophysical Research Letters*, *32*(19). doi:10.1029/2005GL023635

Shi, Z.H., Fang, N.F., Wu, F.Z., Wang, L., Yue, B.J., & Wu, G.L. (2012). Soil erosion processes and sediment sorting associated with transport mechanisms on steep slopes. *Journal of Hydrology*, *454*, 123–130. doi:10.1016/j.jhydrol.2012.06.004

Sun, H., Cornish, P.S., & Daniell, T.M. (2002). Contour-based digital elevation modeling of watershed erosion and sedimentation: Erosion and sedimentation estimation tool (EROSET). *Water Resources Research*, *38*(11). doi:10.1029/2001WR000960

Van der Knijff, J.M.F., Jones, R.J.A., & Montanarella, L. (1999). *Soil erosion risk assessment in Italy*. European Soil Bureau, European Commission, Luxembourg.

Verheijen, F.G., Jones, R.J., Rickson, R.J., & Smith, C.J. (2009). Tolerable versus actual soil erosion rates in Europe. *Earth-Science Reviews*, *94*(1–4), 23–38. doi:10.1016/j.earscirev.2009.02.003

Viney, N.R., & Sivapalan, M. (1999). A conceptual model of sediment transport: Application to the Avon River Basin in Western Australia. *Hydrological Processes*, *13*(5), 727–743. doi:10.1002/(ISSN)1099-1085

Vrieling, A. (2006). Satellite remote sensing for water erosion assessment: A review. *Catena*, *65*(1), 2–18. doi:10.1016/j.catena.2005.10.005

USDA, United States Department of Agriculture. Rainfall Intensity Summarization Tool (RIST 3.98) (2018). Accessed from http://www.ars.usda.gov/News/docs.htm?docid=3251.

Williams, J.R. (1975). Sediment yield prediction with universal equation using runoff energy factor. Present and prospective technology for predicting sediment yields and sources. ARS-S-40. In *US department of agriculture - agricultural research service* (pp. 244–252). Washington, DC: Government Printers.

Wischmeier, W.H., & Smith, D.D. (1978). Predicting rainfall erosion losses-a guide to conservation planning. *Predicting rainfall erosion losses-a guide to conservation planning*. In *USDA agricultural handbook* (Vol. 537, pp. 58). Washington, DC: Government Printers.

Yang, C.T. (1972). Unit stream power and sediment transport. *Journal of the Hydraulics Division*, *98*(10), 1805–1826.

Yang, C.T. (1973). Incipient motion and sediment transport. *Journal of the Hydraulics Division*, *99*(10), 1679–1704.

Young, R.A., Onstad, C.A., Bosch, D.D., & Anderson, W.P. (1989). AGNPS: A nonpoint-source pollution model for evaluating agricultural watersheds. *Journal of Soil and Water Conservation*, *44*(2), 168–173.